UNIVERSITY OF CAMBRIDGE
Department of Engineering

High Early Strength Foamed Concrete

Author Name: Alex Hearne

Supervisor: Professor Abir Al-Tabbaa

Date: 25/05/2016

I hereby declare that, except where specifically indicated, the work submitted herein is my own original work.

Signed ____ *date* ____________________________

High Early Strength Foamed Concrete
Technical Abstract report
Alex Hearne, St John's College

Foamed concrete is a lightweight, highly workable and self-compacting material, with excellent thermal insulation and fire resistance properties. As such, it is highly attractive to the construction industry, and extensively used in applications of void filling and insulation components. However, foamed concrete's low compressive strength has restricted its use in structural load-bearing applications, whilst high shrinkage strains have promoted cracking, warping and joint spalling. This study therefore investigated how to improve compressive strength and autogenous shrinkage of low density foamed concrete. In particular, the study focussed on optimising early compressive strengths, since this is of considerable interest in the construction industry for accelerating construction times. Criteria from Laing O'Rourke were used to provide target values for the properties investigated.

Foamed concrete was produced by entraining a stable pre-formed foam into cement mortar. The volume of foam entrained, typically 40 – 60% by volume, was the primary control of density, and led to a uniform distribution of air voids throughout the mix. Nine foamed concrete mixes were assessed: three different compositions, each produced at densities of 400, 600 and 800 kg/m^3. The first composition used a binder of 100% OPC, the second involved OPC replacement by silica fume, and the third used a superplasticizer in addition to silica fume and OPC. Silica fume undergoes a rapid pozzolanic reaction, which enhances early strength development, whilst superplasticizers allow the reduction of the water/binder ratio.

Compressive strength tests were performed at 1, 7 and 28 days to assess the impact of silica fume and superplasticizer addition on early and long-term strength, whilst shrinkage samples were tested at more regular intervals varying from 1 to 4 days.

It was found that cement replacement by silica fume increases early strength for a given density, but reduces long-term strength relative to OPC mixes. The addition of a superplasticizer provided the greatest early and long-term strengths at all densities due to the increased cement content from a reduction in water/binder ratio.

Compressive strength increased approximately exponentially with density for all mix compositions. Strength variation between mixes also appeared to increase with density. It

thus follows that density has the greatest influence on strength, and considerably more than the effect of composition at low densities. Closer assessment of void structures showed that higher density mixes exhibited both narrower voids and a more uniform distribution throughout the sample – existing literature has also indicated that both factors contribute to higher strengths. Mix composition did not appear to affect void distribution.

Feret's model was shown to provide an accurate prediction of compressive strength for all mix compositions based on volumetric proportions of cement, water and air. The unknown values from Feret's model, dependent on the mix composition, were evaluated to provide the best fit of the curve through the data, along with an associated R-squared value to quantify the fit. Similarly, Balshin's model relating compressive strength and porosity was shown to be accurate for OPC + SF mixes, but the validity fell away for OPC + SF + SP mixes (OPC = Ordinary Portland Cement, SF = silica fume, SP = superplasticizer).

The addition of silica fume by cement replacement reduced autogenous shrinkage at all densities relative to a pure OPC binder. This suggests that OPC content is a primary factor influencing autogenous shrinkage in foamed concrete. The introduction of a superplasticizer increased autogenous shrinkage due to the reduction in water/binder ratio. However, the shrinkage of OPC + SF + SP mixes remained lower than that of OPC mixes at all densities.

The effect of density showed that autogenous shrinkage was greater at higher densities. Furthermore, the increased shrinkage due to a lower water/binder content appeared more influential at higher densities. This suggests that higher cement content not only increases shrinkage by itself, but also enhances the effect of other factors influencing shrinkage.

This study satisfied Laing O'Rourke's early strength specification for all mixes, whereby at least 25% of long-term strength is developed at 1 day. The long-term strength criterion of 4MPa at 28 days was only satisfied by the OPC + SF + SP mix at 800 kg/m^3, whilst criteria for void size and shrinkage were not satisfied by any mix.

Further work could therefore be carried out to optimise the OPC + SF + SP mix with regard to shrinkage by introducing an expansive agent. The reduction of the water/cement ratio could also be investigated to further increase strength at all densities, but should be considered alongside flowability. Alternatively, a new direction could be taken by investigating the effect of reinforcing fibres or the curing regime on strength and shrinkage.

Contents

1. Introduction 4

1.1 Background and motivation 4

1.2 Project aim 5

2. Literature review 6

2.1 Foamed concrete 6

2.2 Compressive strength 7

2.2.1 Effect of density 7

2.2.2 Effect of silica fume 8

2.2.3 Effect of superplasticizers 9

2.2.4 Other influential factors 10

2.3 Compressive strength prediction models 10

2.4 Drying shrinkage 12

2.4.1 Effect of density 12

2.4.2 Effect of silica fume 12

2.4.3 Effect of superplasticizers 13

2.4.4 Other influential factors 13

2.5 Autogenous shrinkage 13

2.6 Water absorption 15

2.7 Thermal properties 15

3 Materials and methods 16

3.1 Materials 16

3.1.1 Ordinary Portland cement 16

3.1.2 Silica fume 17

3.1.3 Superplasticizers 17

3.2 Mix design 18

3.3 Experimental Technique......19

3.3.1 Foam......19

3.3.2 Mixing and casting......20

3.3.3 Testing......24

4 Results and discussion......27

4.1 Compressive strength......27

4.1.2 Effect of density......29

4.1.3 Void structure......31

4.2 Autogenous shrinkage......38

4.2.1 Effect of composition......38

4.2.2 Effect of density......41

5 Conclusions and further work......43

6 References......47

7 Appendix......50

7.1 Risk assessment retrospective......50

Figures

Figure 1: Effect of silica fume addition on compressive strength......9

Figure 2: Effect of superplasticizer addition on the early strength of concrete......10

Figure 3: Effect of silica fume addition on autogenous shrinkage of concrete......14

Figure 4: (a) Propump foam generator; (b) Fresh foam......20

Figure 5: Inclined rotating drum mixer......21

Figure 6: Manufacturing process of foamed concrete......22

Figure 7: (a) Polystyrene mould; (b) Demoulded strength sample......23

Figure 8: EN 12390-4 compression frame 25
Figure 9: Shrinkage apparatus 26
Figure 10: Compressive strength vs Density..27
Figure 11: Compressive strength vs Time..27
Figure 12: Compressive strength vs Feret's parameter..30
Figure 13: Schematic of location of sampling areas across cube cross-section 31
Figure 14: Compressive strength vs porosity..34
Figure 15: Microscope images of the mixes' void structure..37
Figure 16: Autogenous shrinkage strain vs time at each density 38
Figure 17: Autogenous shrinkage strain vs time 41
Figure 18: 28-day shrinkage vs porosity for all mixes..42

Tables

Table 1: Mix compositions 19
Table 2: Values of K and R-squared for Feret plots 30
Table 3: Statistical analysis of void size and distribution..32
Table 4: Porosity calculations 34
Table 5: Values of σ, b, and R-squared for Balshin plots..35
Table 6: Compliance with LOR's specification. 44

Introduction

1.1 Background and motivation

Over 3 billion tonnes of cement are produced each year [1], making concrete one of the most utilized substances on Earth, second only to water. Such extensive use stems from its advantageous properties of high strength, durability and versatility across a broad range of construction applications, including buildings, bridges, tunnels and roads. However, there is considerable concern over the environmental impact of such large use, and most notably from the production of cement, the primary constituent of ordinary concrete. Cement production has been estimated to contribute 5% of annual global man-made CO_2 emissions [2], greater than the entire aviation industry. The viability of foamed concrete as an alternative to ordinary concrete for certain applications has thus been proposed, since it offers a sustainable and innovative solution.

Investigation into foamed concrete originally dates back to 1923, although detailed assessment of production techniques, composition and engineering properties began in 1954. Its application in commercial use was only recognised in the late 1970s, with void filling and ground stabilisation in The Netherlands, but considerable improvements in production methods and foaming agents have stimulated greater production and interest in foam concrete's potential for a wide range of applications [3]. Foamed concrete consists of the same materials as ordinary concrete, including cement and water, but uses foam as a replacement for aggregate. This allows foam concrete's characteristically low densities of 400 – 1600 kg/m^3 to be achieved [1], considerably lighter than ordinary concrete.

In structural elements, the replacement of ordinary concrete with foamed concrete can significantly reduce dead weight to reduce the loading on columns and foundations. Furthermore, the improved strength/weight ratio allows reinforced foamed concrete beams to span over greater distances. Therefore, the combined reduction in required load bearing material can both accelerate the construction process and provide huge cost savings, whilst also offering a 'greener' solution with lower embodied carbon.

At the lower range of densities, foamed concrete's applications typically include thermal and sound insulation, void filling and fire resistance. It is therefore of interest to assess the limit of foamed concrete's structural load-bearing properties at low densities, to assess if these applications can be combined in secondary structural applications.

The speed and efficiency requirements of the construction industry dictate that early strength development is highly advantageous: foamed concrete with high early strength allows faster construction time through accelerated formwork rotation. Furthermore, with high early strength development, foamed concrete can be employed at far lower temperatures, and so may be more suitable in extreme climates.

The development of a lightweight foamed concrete with high early strength would therefore provide a quicker and cost effective solution to the typical foamed concrete applications of void filling and insulation components. Indeed, its use in emergency void filling is particularly important, where it is required to quickly stabilise the ground by providing support as well as filling the void. The value of rapid early strength development is also shown in relief uses such as temporary shelters required following natural disasters. High early strength foamed concrete would provide a sustainable and thermally efficient material that could be constructed rapidly and economically.

1.2 Project aim

This work aims to investigate how the composition of foamed concrete affects early strength and shrinkage at differing low densities.

The foam content was varied to produce cubes of different densities, and the composition varied with the use of silica fume and a superplasticizer to increase 1-day strength at each density. Shrinkage was also assessed and optimized.

This work is sponsored by Laing O'Rourke ('LOR'), which provided the following target specifications for foamed concrete properties:

1. Density < 800 kg/m^3
2. Long-term strength > 4 MPa
3. Void size < 0.5mm
4. Lightly expansive ≈ 0.5%
5. > 25% long-term strength after 20 hours at 20°C
6. Closed voids for low water absorption

1. Literature review

2.1 Foamed concrete

Foamed concrete is commonly defined as ‘a cementitious material having a minimum of 20 per cent by volume of mechanically entrained foam in the plastic mortar or grout’ [1]. The composition of foamed concrete includes cement, sand, water and a pre-formed foam, and so differs from ordinary concrete, since coarse aggregates are replaced with pre-formed foam. At low density sand is typically omitted, whilst Supplementary Cementitious Materials can be used to replace proportions of cement and vary the overall properties of the mix.

The production of foamed concrete is performed by mixing cement slurry with pre-formed foam. Pre-formed foam itself is extremely stable, created from the addition of a foaming agent with water and compressed air, and is blended with the mortar in a mixer. Typically, foamed concrete can be made to dry densities of 300 – 1600 kg/m^3 and 28-day compressive strengths of 0.2 – 10 MPa [1].

Foamed concrete is self-compacting, highly flowable under self-weight and pumpable over long distances, and so provides excellent void filling solutions. Indeed, its traditional use was trench reinstatement, since foamed concrete provides good load spreading characteristics, and the ease of production means it is cost-effective. Void filling has since been extended to a wide range of scenarios, including wells, tunnels and storage tanks, and can be either planned or used in emergencies, where rapid stability and support are required.

The porous microstructure of foamed concrete, with many discontinuous voids, provides excellent thermal insulation properties. With low self-weight, foamed concrete is widely used for insulation components in walls, floors and roofs. This void structure also provides beneficial durability properties over normal weight concrete. Indeed, foamed concrete has become particularly popular in the Middle East, where it is used to negate the effects of earthquakes and large temperature changes [4]. Excellent fire resistance properties have been exhibited: in the presence of intense heat, foamed concrete does not spall or explode, unlike normal weight concrete [5]. Furthermore, water absorption is low, providing strong resistance to the freeze-thaw cycle.

Further uses have included road sub-bases in low loading scenarios, soil stabilization and bridge abutments, where significant costs savings can be made with reduced foundation size and wall thicknesses. Less commonly, foamed concrete has also been used for shock absorbing barriers for airports and traffic [4].

The drive for sustainability and reduced environmental impact in the construction industry makes foamed concrete a hugely exciting material. Significant energy savings are made through cement replacement by Supplementary Cementitious Materials, and the removal of aggregates, which require energy-intensive quarrying.

2.2 Compressive strength

2.2.1 Effect of density

Kearsley found that compressive strength of foamed concrete increased exponentially with density for mixes above 900kg/m^3 [6]. The study varied density using the air/cement ratio, and showed that whilst strength reduces with increasing air/cement ratio, the effect is less influential at lower densities and lower compressive strengths.

At lower densities, between 500 – 1000 kg/m^3, closer analysis revealed that the size of void diameter is the primary factor influencing strength [7]. Nambiar and Ramamurthy analysed this effect by comparing the effects of void size parameters D50 and D90 on strength [8]. Through statistical analysis, D90 was shown to correlate more closely with strength than D50, with R-squared statistics considerably higher. This suggests that it is the larger voids that have the greatest influence on strength.

Furthermore, D90 was shown to increase more quickly with foam volume than D50, and resulted in the curves of D50 and D90 converging at lower densities, indicating that voids become both narrower and more uniform at lower densities. Such rapid increase of larger voids with lower density is from increasing coalescence, which leads to larger variation in void diameters and subsequently lower strength.

Above 1000kg/m^3, the void diameter had less of an impact since the void spacing was high and distribution more uniform, and paste composition was found to be more influential [7].

2.2.2 Effect of silica fume

Cement replacement by silica fume has been shown to increase strengths at high densities [9]. Since silica fume has a specific gravity less than that of Portland cement, its use as a replacement material can reduce foam volume for the same density, leading to greater strengths. Furthermore, due to its fineness of particles, silica fume's use as a filler has decreased void sizes and provided a more uniform void distribution within the paste [10, 11]. As described above, this effect increases compressive strength.

In particular, the addition of silica fume as a cement replacement has been shown to have its greatest impact through increasing *early* strength of foamed concrete. High density samples (800kg/m^3 – 1500kg/m^3) containing no silica fume developed only 70 – 75% of 28-day strength after 7 days, whilst those with 6% (by weight) silica fume developed 85 – 90% [12]. The initial strength gain comes from the rapid pozzolanic reaction of silica fume with calcium hydroxide in the cement paste to form CSH, the primary strength constituent in cements: half of the silica fume typically reacts within 1 day, and two-thirds within the first 3 days [13].

The strength enhancement of silica fume is typically more pronounced at higher densities, with greater paste content [6, 14]. Kearsley's plot relating compressive strength, silica fume addition and foam volume [6], shown below in Figure 1, clearly shows this with increased strength enhancement at lower foam volume (higher densities). Indeed, for very low density mixes, with foam volumes of 60%, Kearsley found no strength enhancement at any percentage of silica fume addition.

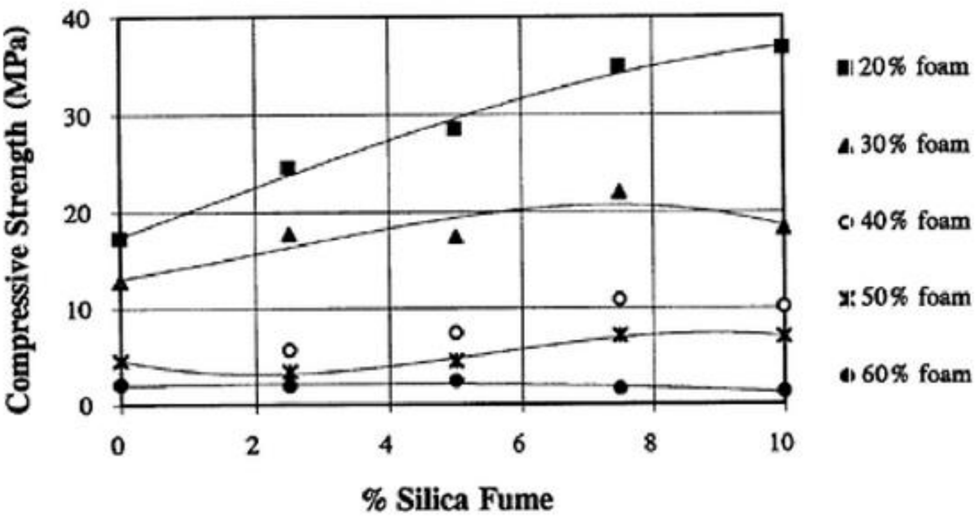

Figure 1: The effect of silica fume addition on compressive strength at different foam contents [6]

2.2.3 Effect of superplasticizers

Several studies have shown the addition of a superplasticizer can increase compressive strength in foamed concrete [3, 10, 14]. The water-reducing nature of superplasticizers mean that cement hydration requires less water, and the water/cement ratio can therefore be reduced. This allows greater cement content for a given density, which increases compressive strength [3]. Indeed, the same effect is seen in ordinary concrete, where Neville observed that reductions in water/cement ratio, whilst ensuring sufficient water for hydration, can enhance early strength by 50 – 75% [13]. Neville's results are shown below in Figure 2. This effect will, however, only increase strength if sufficient water is available for hydration - should the water content be too low, the mix is too stiff and could cause bubbles to break. Conversely, if water content is too high, the paste may be too thin and lead to segregation [10].

A notable issue with superplasticizers is incompatibility with binder constituents, which leads to foam instability [14]. As such, the composition of superplasticizer must be carefully chosen to ensure a stable mix.

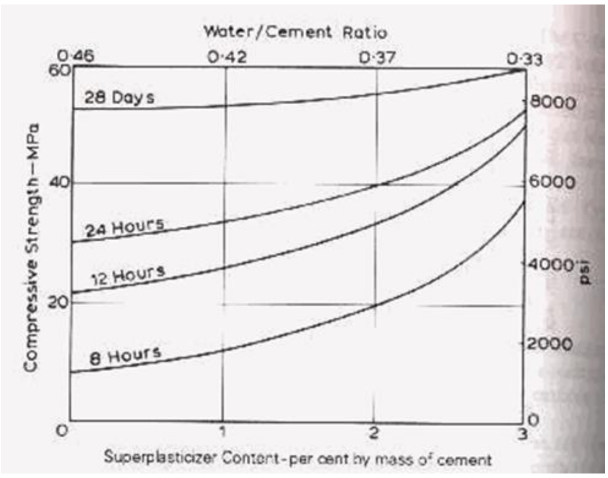

Figure 2: Effect of superplasticizer addition on the early strength of concrete [13]

2.2.4 Other influential factors

Kearsley and Wainwright [15] assessed the impact of cement replacement by large volumes of fly ash at high densities of 1000 – 1500kg/m^3. It was found that up to 67% of cement could be replaced by fly ash without significant reduction in strength. However, the results showed that strength contribution from fly ash delays strength development in a mix. Fly ash itself is not a cementitious material, but when reacted with calcium hydroxide it produces compounds with cementitious properties. This reaction therefore delays strength contribution.

The effect of varying curing regimes on foamed concrete compressive strength has also been studied [16]. Foamed concrete of density 1200 – 1600kg/m^3 was analysed, with results showing that moisture curing produced greater 28-day strengths than both water and air curing.

2.3 Compressive strength prediction models

Several compressive strength prediction models have been proposed and validated. Hoff [17] proposed the strength-porosity relationship for foamed concrete consisting of only air, water and cement:

$$\frac{\sigma_y}{\sigma_0} = \left(\frac{d_c}{1+k}\right)^b \left(\frac{1+0.2\rho_c}{\rho_c \gamma_w}\right)^b \qquad (1)$$

where σ_y is the predicted compressive strength, σ_0 is the theoretical compressive cement paste strength at zero porosity, d_c is the concrete density, ρ_c is the specific gravity of cement, k is the water/cement ratio (by weight), γ_w is the unit weight of water and b is an empirical constant.

Hoff's formula is a generalised form of Balshin's [18] model, $\sigma_y = \sigma_0(1-n)^b$, where n is porosity. The theoretical porosity is generated by Hoff by assuming total void space as the evaporable water space plus the air void space, and using a value of 0.2 for the ratio of water bound by hydration to cement. A clear deficiency of the model is that the effect of pore size is not considered, since the same porosity can be achieved for many small voids or fewer larger voids, where the latter typically reduces strength capacity [17].

Following experimental analysis using a range of cement types, Hoff formulated appropriate values of σ_0 ranging from 115 – 290 MPa, and of b from 2.7 – 3.0. Using these values, the range of predicted compressive strengths for mixes with 100% OPC binder can be calculated. For the prescribed densities of 400, 600 and 800kg/m^3, this gave 0.55 – 0.76MPa, 1.64 – 2.57MPa and 3.55 – 6.10MPa respectively.

Kearsley and Wainwright [19] extended Balshin's model to foamed concrete with cement replacement by both classified and unclassified fly ash, showing compressive strength to be a function of both porosity and age. A multiplicative model provided the best fit to experimental data:

$$\sigma_y = 39.6(\ln t)^{1.174}(1-p)^{3.6} \tag{2}$$

Here, t is time since casting in days and p is the mature porosity measured after 365 days. The theoretical compressive cement paste strength at zero porosity, σ_0, has been expanded to account for variability with time up to one year since casting, at which point it is assumed to remain constant, as in Balshin's model.

Further work has related strength and volumetric composition. Tam et al. used Feret's model [20] to incorporate the volumetric proportions of cement, water and air:

$$\sigma_y = K\left(\frac{c}{c+w+a}\right)^n \tag{3}$$

where c, w and a are the absolute volumetric proportions of cement, water and air, and K and n are empirical constants. Adaptations of this model have incorporated the degree of hydration, which has further improved the correlation of volumetric composition and compressive strength. For the purpose of this study, Tam et al.'s model will be used since the degree of hydration is unknown. The value of n=2 is used in later analysis, on recommendation for normal-weight concrete [20].

2.4 Drying shrinkage

2.4.1 Effect of density

Drying shrinkage has proved a significant problem in foamed concrete at high densities, where samples have been shown to shrink between 0.1 – 0.3% [21]. This is approximately 4 – 10 times the shrinkage of regular concrete of the same density [21]. Foamed concrete undergoes such high drying shrinkage due to high cement content and high water content, but also the lack of coarse aggregates, which restrain shrinkage locally in normal concrete. Furthermore, Jones and McCarthy showed that drying shrinkage is highly related to density, with lower shrinkage at lower densities [22]. This is because, for a given water/cement ratio, higher density mixes have greater cement content to undergo shrinkage. Therefore, there is greater free water volume, increasing the amount available for evaporation and thus greater shrinkage. In addition, Ziembicka showed that drying shrinkage is also a function of the volume and specific surface of micropores [23]: drying shrinkage increased with either a decrease in void diameter, or an increase in the number of small pores.

Where drying shrinkage may be expected to be large, curing by autoclaving has reportedly decreased the effect by 12 – 50% of that of moist-cured concrete [24]. Ramamurthy and Narayanan suggested that the reduction due to autoclaving implied that drying shrinkage is heavily influenced by the physical structure of the hydration product [25].

2.4.2 Effect of silica fume

Cement replacement by silica fume has been shown to have a small effect in increasing shrinkage in foamed concrete [25]. The fine silica fume particles increase the formation of microcapillaries [26], resulting in a greater number of small voids. This therefore increases drying shrinkage, which is in line with the observations of Ziembicka [23].

2.4.3 Effect of superplasticizers

The addition of superplasticizers to a mix composition has not been found to have a significant effect on shrinkage, providing the water/cement ratio is reduced appropriately [3]. For a given water/cement ratio, the water-reducing nature of superplasticizers results in a greater free water content. This increases drying shrinkage since more water is lost from pores. Therefore, for a given dose of superplasticizer, the water/cement ratio must be adjusted appropriately to prevent additional drying shrinkage. Kearsley demonstrated this effect by reducing the water content for foamed concrete mixes composed of cement, fly ash and silica fume accompanied with a superplasticizer [6].

2.4.4 Other influential factors

Drying shrinkage has been shown to increase with increasing percentages of fly ash in foamed concrete [27]. Samples of 1500 kg/m^3 were varied in binder composition by up to 60% cement replacement of fly ash, which exhibited a microstrain of 1128, the highest of all samples. Fly ash is expected to increase shrinkage in a similar way to silica fume, since finer particles induce smaller voids, which is associated with higher drying shrinkage [23].

The use of lightweight aggregate has been shown to reduce drying shrinkage [28], since they provide rigidity to the matrix, which is absent for binders containing only finer particles.

2.5 Autogenous shrinkage

When considering the applications of foamed concrete, only a small fraction of the material will be exposed to air and thus undergo drying shrinkage. Indeed in applications such as void filling, much of the surface will be coincident with impermeable surfaces. The majority of foamed concrete is therefore subject to sealed conditions and, as such, it is more appropriate to consider the effects of autogenous shrinkage. There is, to date, no literature on autogenous shrinkage of foamed concrete, but analysis of autogenous shrinkage of normal concrete can give indications of the performance of foamed concrete cement paste.

Neville states that autogenous shrinkage strain in normal concrete is approximately 40 x 10^{-6} at one month curing [13]. This is likely to be an order of magnitude smaller than that of foamed concrete cement paste due to the absence of aggregates. As with drying shrinkage, autogenous shrinkage was found to increase with density, due to increased cement paste content [13, 29].

Studies of ordinary Portland cement concrete showed that autogenous shrinkage is only prominent at low w/c ratios [30], and that it increases with a decrease in w/c ratio and an increase in silica fume content [31]. Neville states the increase due to a reduction in w/c ratio may be due to increased self-desiccation – the use of free water in hydration such that there is insufficient water to cover the surfaces of unhydrated particles, or maintain 100% humidity within the concrete system [13]. This increases capillary tension of the pore water, leading to greater autogenous shrinkage. Increased shrinkage due to silica fume addition results from the fine particles of silica fume, which produce a narrower pore size distribution. The narrower pores induce greater capillary tension and hence greater autogenous shrinkage [30]. Figure 3 below demonstrates this effect for normal concrete.

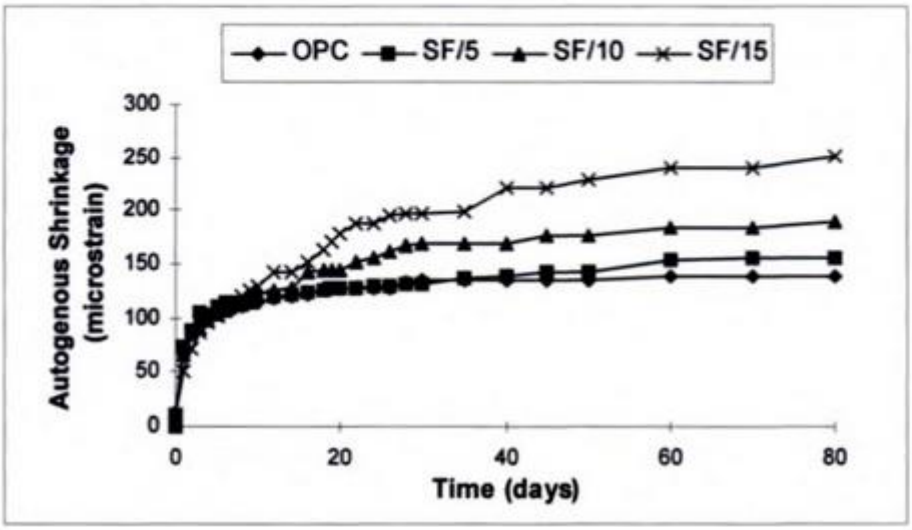

Figure 3: *The effect of silica fume addition on autogenous shrinkage of concrete*

2.6 Water absorption

Water absorption of foamed concrete has been shown to be primarily a function of paste content [10], increasing with at greater densities. Whilst not all artificial pores affect water absorption, since they are not interconnected, it is the greater capillary pore volume from increased paste content that results in greater water absorption.

2.7 Thermal properties

Foamed concrete's cellular microstructure provides significant benefits for thermal applications, such as insulation. Foamed concrete of 1000kg/m^3 was observed to have a thermal conductivity one-sixth of the value of typical cement-sand mortar at the same density [32]. Furthermore, density appears to be the key factor influencing insulation [33]: a decrease in density of 100 kg/m^3 reduced the thermal conductivity of lightweight aggregate foamed concrete by 0.04W/mK [34].

Foamed concrete also possesses superior fire resistance properties than normal concrete. Jones and McCarthy observed that low density foamed concrete underwent less strength loss in fire than normal concrete [35]. Valore suggested this was due to the effects of radiation heat transfer through a porous material at high temperatures [36]. Radiation heat transfer is inversely related to the number of air-solid surfaces in a material, and so greater porosity provides greater resistance.

3 Materials and methods

3.1 Materials

3.1.1 Ordinary Portland cement

Ordinary Portland Cement (OPC) is the fundamental ingredient in concrete, and dictates many of its properties. OPC is a fine powder, produced by heating a mixture of limestone and clay at high temperatures, before grinding it to a fine powder and adding gypsum.

The two key reactions which occur during the hydration of Portland cement involve the anhydrous compounds calcium silicates and calcium aluminates. The first is the hydration of Tricalcium Aluminate, C_3A, which occurs rapidly over the first 4 hours, and causes the cement to set and harden quickly. The addition of gypsum is used for retardation and helps to prevent a flash set.

The second is the hydration of Dicalcium silicate, C_2S, and Tricalcium Silicate, C_3S, to form Calcium Silicate Hydrate (CSH) gel. CSH provides the main binding material within the matrix, occupying approximately 50% of cement paste volume. In particular, the reaction of C_3S occurs rapidly, and is almost entirely responsible for early strength development. C_2S, conversely, hydrates comparatively slowly and provides less strength contribution, which only proves significant after approximately 7 days. Whilst much of the ultimate strength is gained within the first 28 days, these reactions continue for many years and so provide continued, but decreasing, strength gain in the long-term.

The formation of CSH gel significantly increases the solid volume phase as water is used in hydration. The capillary pore system consequently reduces in volume and may become discontinuous, leading to a considerable reduction in permeability.

The environmental impact of manufacturing Portland cement has been seen as one of its key challenges. The process requires considerable energy consumption, with production of one ton of Portland cement shown to produce approximately one ton of CO_2 and other greenhouse gases [37]. As such, in order to reduce the embodied carbon of concrete, significant work has focussed on replacing proportions of Portland cement with Supplementary Cementitious Materials, such as silica fume, fly ash and ground-granulated blast-furnace slag (GGBS).

3.1.2 Silica fume

Silica fume is a very fine, highly reactive pozzolan with very high amorphous silicon dioxide content. It is a by-product from the production of silicon metal of ferrosilicon alloys.

Along with CSH, another product in the hydration of Portland cement is calcium hydroxide, CH, which typically provides a source of weakness for crack propagation, and thus greatly limits strength. Silica fume reacts with CH to produce CSH, in addition to the CSH produced through the original hydration of Portland cement. The generation of additional CSH therefore improves compressive strength. The reaction of silica fume with CH occurs rapidly, and thus accelerates setting and strength gain. The early strength development is a key property of silica fume which this study aims to utilise.

The fineness of particles, typically 100 times smaller than ordinary Portland cement [38], allow silica fume to act as a filler, providing a denser matrix and reducing void size. According to literature, the narrower void size typically enhances compressive strength [39]. Furthermore, the narrower void size means that the void structure is more discontinuous, which has the result of reducing permeability.

3.1.3 Superplasticizers

Superplasticizers are chemical admixtures, typically used as high-range water reducers, due to their effective plasticising effects. Classed as organic polymers, superplasticizers increase the workability of concrete by separating cement particles and the water content of the mix. This is done by neutralizing the ionic charge of the cement particles, thus allowing the cement to flow more freely whilst bound with less water.

Therefore, for a given workability, the use of superplasticizers allows the reduction of the water/binder ratio by 12 – 30% [40], whilst maintaining the same workability of the mix. As shown in literature, the reduction in water/binder ratio increases the strength of foamed concrete [41]. In the same way, for a given strength, the workability of a mix can be significantly improved by adding a superplasticizer.

However, care should be taken with the addition of superplasticizers, since enhancements in workability are typically short lived. Rapid slump loss can occur, which can be as great as to neutralise any initial gain in workability. This has implications for industry, particularly in applications involving long transportation times.

Application dosages vary between 0.5 – 3% by weight of cement [42], depending on the superplasticizer employed and its compatibility with the mix constituents. The superplasticizer used in this study is Sika® ViscoCrete® 10, which has a recommended dosage of 0.2 – 1.5% by weight of cement.

3.2 Mix design

The proportions of constituents required for each mix are calculated from the sum of their masses within a unit volume. The foam is considered weightless, as recommended by The Concrete Society [1], and so the target wet density (D, kg/m^3) is the sum of binder content (c, kg/m^3) and water content (w, kg/m^3). Using the water/binder ratio (w/c), the individual weights of the binder and water per m^3 can be found, and subsequently converted to volumes using their respective densities. The remaining volume within the m^3 is attributed to foam volume (V_{foam}, m^3). These values are then scaled depending on the required concrete volume.

$$\text{Target wet density, } D = c + w \quad (4)$$

$$\text{From literature recommendation [43], } w = c/2 \quad (5)$$

This now provides the weights of binder constituents.

$$\text{Volume of foam, } V_{foam} = 1 - \frac{c}{3150} - \frac{w}{1000} \quad (6)$$

where 3150 and 1000 kg/m^3 are the densities of cement and water respectively. The process above assumes a binder of 100% cement. When binders are composed of multiple constituents, assuming their proportions and densities are known, a similar process to that above can then be followed, allowing for the additional terms.

Existing literature has stated the importance of the water/binder ratio in achieving a stable mix. Excess water content may lead to unstable foam; insufficient water content may prevent the foam blending with the paste. The ratio has been established empirically to be between 0.4 and 1.25 [43]. Since lower values induce greater compressive strength, a value of 0.5 is used in this study for OPC and OPC + SF mixes. The addition of a superplasticizer allows the water/binder ratio to be reduced, and hence a value of 0.4 is used for OPC + SF + SP mixes.

The full outline of mixes assessed in this investigation, including composition proportions and water/binder ratios, are detailed below in Table 1. The proportion of silica fume was selected on assessment of its previous use in literature.

Mix	Density (kg/m^3)	W/B ratio	OPC (kg/m^3)	SF (kg/m^3)	Viscocrete (kg/m^3)	Foam Volume (litres/m^3)
AHOPC7	400	0.5	400	-	-	780
AHOPC8	600	0.5	400	-	-	670
AHOPC9	800	0.5	400	-	-	560
AHSF10	400	0.5	360	40	-	780
AHSF11	600	0.5	540	60	-	670
AHSF12	800	0.5	720	80	-	550
AHSP13	400	0.4	358	40	2	790
AHSP14	600	0.4	537	60	3	680
AHSP15	800	0.4	716	80	4	580

Table 1: Densities and mix proportions by weights of constituents

For later reference, the discussion of all densities referring to one mix composition will be denoted with a dash. For example, AHSP13 – 15 refers to AHSP13, AHSP14 and AHSP15. The mix composition (e.g. OPC + SF + SP) is often also included for clarity.

3.3 Experimental Technique

3.3.1 Foam

Foam was generated using a Propump Limited Engineering JFG 200 foam generator, shown in Figure 4(a) with the resulting foam in Figure 4(b). This involved feeding compressed air and a solution of foaming agent into the generator, which forces the mixture through a plastic mesh to produce foam. Compressed air was inputted at a pressure of 0.8MPa, whilst the foaming agent solution had a concentration of 40ml per litre of water, since these values were found to produce consistent foam. The foaming agent used was protein-based, since this provides greater strength performance than synthetic-based foaming agents, despite being more expensive and energy-intensive in production [1].

This is known as the ‘dry’ method of foam production, which is recommended for low density foamed concrete [44], since it produces more stable foam than ‘wet’ foam production. Furthermore, dry foam bubbles are smaller than those of wet foam, at less than 1mm diameter, and more uniformly sized throughout the foam. According to literature, this improves strength in foamed concrete.

(a)

(b)

Figure 4: (a) Propump foam generator; (b) Fresh foam

3.3.2 Mixing and casting

The mix procedure began with the calculation of the weight of mix constituents and volume of foam according to the ‘Mix Design’ process described earlier. Each mix constituent was then weighed out and the dry binder constituents placed into an inclined rotating drum mixer, shown in Figure 5. The mixer was chosen due to its consistent mixing action which aided homogeneity within the mix.

Figure 5: *Inclined rotating drum mixer*

The dry binder constituents were mixed for 30 seconds to ensure a uniform distribution of any cement replacement materials, before water was added at intervals, again to aid consistency. Mixing occurred for a further 2 minutes, stopping at 30 second intervals to check no dry binder particles remained adhered to the sides of the drum.

The next stage was to produce the correct volume of foam using the foam generator, ensuring good stability and consistency. All foam would then be added to the cement mortar slurry at once and mixing continued until the liquid foamed concrete appeared to be of a uniform texture. This typically took an additional 3 minutes.

The full manufacturing process is outlined schematically in Figure 6 below.

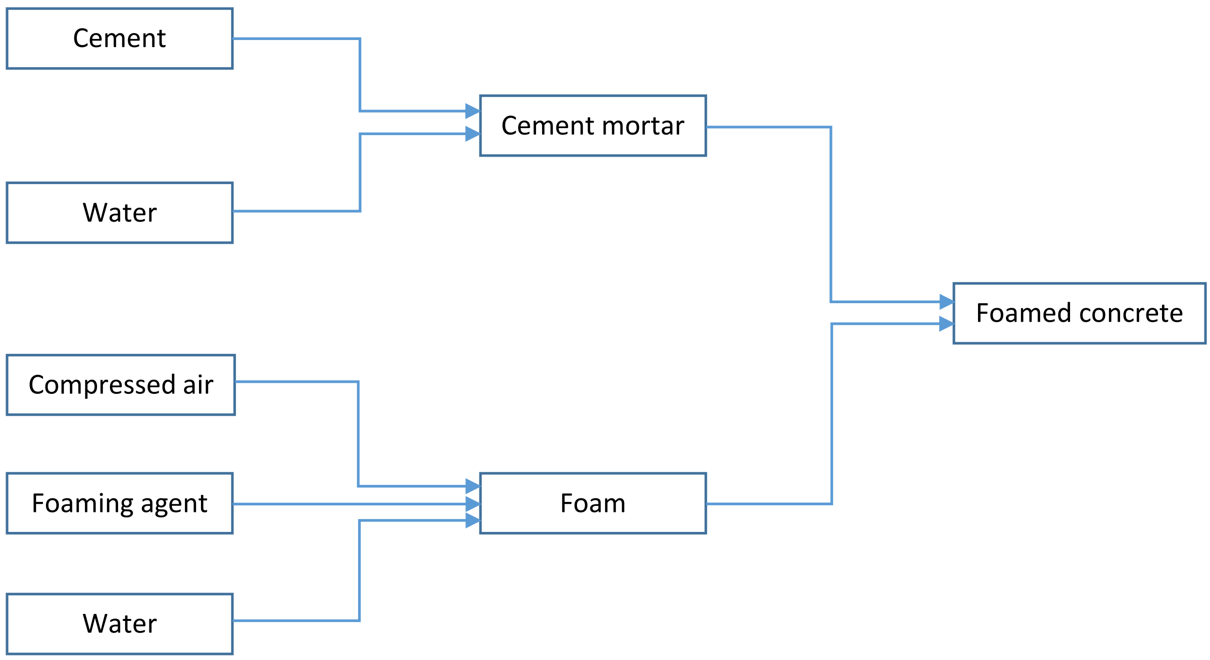

Figure 6: Manufacturing process of foamed concrete

When ready for pouring, the mix was placed into ten 100 x 100 x 100mm cubic polystyrene moulds, and three 500 x 100 x 100mm shrinkage prisms.

Polystyrene moulds were used to ease demoulding – polystyrene can be peeled off, preventing damage of mixes at one day, which can be brittle. The excellent insulation properties of polystyrene ensure a constant temperature is maintained at the cube surface, and ensures good hydration. Polystyrene is also effective in restricting moisture transfer with surroundings, which is important for hydration, although occasionally very small amounts of mix water were observed below cubes upon demoulding.

Shrinkage prisms were composed of steel, since these provided the structural properties that allowed the end pins to set fully immersed within the concrete. The rigidity of the pins was crucial, since they provide the point of measurement for the displacement gauge. Vibration was not required upon pouring, since foamed concrete is self-compacting and self-levelling, although a trowel was required in some cases to smooth top surfaces and ensure correct volumes within each mould.

The fresh density of each cube was then obtained by weighing each cube, and deducting the weight of the mould. Following this, strength moulds were sealed with a top polystyrene cover, and shrinkage moulds covered with polymer bags to prevent moisture transfer (replicating autogenous shrinkage), before being left to set at room temperature.

Demoulding was performed after 24 hours, at which point sufficient hydration had occurred for demoulding to occur without damage of specimens. Dry densities could then be calculated, and shown, ideally, to be within the specified tolerance of the target density. This tolerance was taken as 50 kg/m^3, which is in line with industry production standards [35]. Figure 7 below shows strength samples before, (a), and after, (b), demoulding.

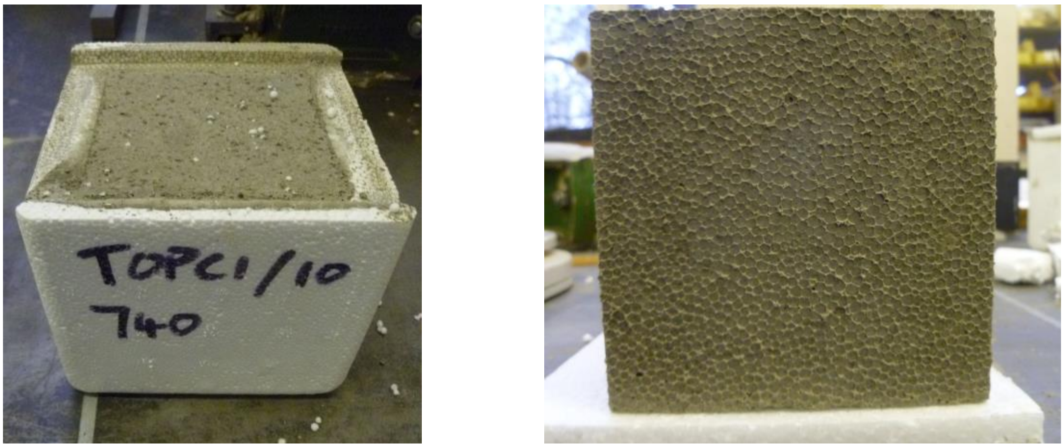

(a) *(b)*

Figure 7: (a) Polystyrene mould containing hardened strength sample, prior to demoulding; (b) Demoulded strength sample

At this point, one of the ten cubes would be discarded. This would be chosen as the cube with either visible defects or a density significantly different from the target density. The nine remaining cubes were then separated into groups of 3 and placed into polymer bags, with each group to be tested at 1, 7 or 28 days. Cube groups were chosen to have an average density as close as possible to the target density to provide consistency at each testing time.

Shrinkage specimens required careful demoulding due to concrete adhesion with the steel mould. Following this they were wrapped with aluminium tape to provide an impermeable boundary, preventing moisture transfer with surroundings and replicating autogenous shrinkage. Testing was performed at intervals of 1 – 4 days.

Samples were then left to set in a room of temperature 19±2°C and relative humidity 50±10%, and tested at their prescribed time intervals.

3.3.3 Testing

Density

Plastic density was measured in accordance with BS EN 12350-6, where samples were weighed in a pre-weighed container of known volume. Two values were recorded for each cube – a 'wet' density directly following placement into moulds and a 'dry' density directly following demoulding.

Wet density proved difficult to predict accurately using the target density, since a number of factors produce varied results. During mixing, the interaction of foam with cement constituents may result in either expansion or contraction depending on the chemical reactions taking place. Trial mixes were therefore performed in order to check the compatibility of the foam with the mix constituents. Furthermore, the mixing process causes foam bubbles to collapse and results in a loss of foam volume. This leaves an insufficient volume of foam required for the target density, which is thus rendered an underestimate. Following this observation, it was found that using a target density of approximately 20kg/m^3 greater than that required was sufficient to achieve the correct wet density.

In addition, dry density was also found to lower than wet density. This is due to moisture loss occurring in the 24 hours prior to demoulding, since the polystyrene moulds were not perfectly impermeable. The decrease from wet density to dry density was found to be dependent on target density, where a lower drop would be observed for lower densities. Mixes in this investigation showed a drop of 20 – 50kg/m^3, but this has been as great as 80kg/m^3 in literature [45].

Since it is difficult to achieve absolute homogeneity across the mix batch, it was unsurprising that typical variation was 20 – 40kg/m^3, although this is within the tolerances outlined earlier in this section.

Compressive strength

Nine cubes were tested – three at each of the strength testing intervals of 1, 7 and 28 days. Cubes were tested using an EN 12390-4 compression frame, shown below in Figure 8, which has a strength capacity of 250kN (corresponding to 25MPa for our cubes). Of the three readings recorded for each mix at each testing interval, the average was taken as the compressive strength value used for analysis, with the upper and lower values providing observed deviation from the average.

Figure 8: EN 12390-4 compression frame

Shrinkage

For each mix, the three shrinkage samples were measured at daily intervals initially, before a reduction in frequency due to time allowances. Readings were taken using a mechanical displacement gauge, which was calibrated at each testing time using a reference bar. The first reading was taken at 1 day, from which future readings could be measured against to give an absolute change in displacement, and hence shrinkage strain. The average values of the samples for each mix was taken as the recorded shrinkage value at that time.

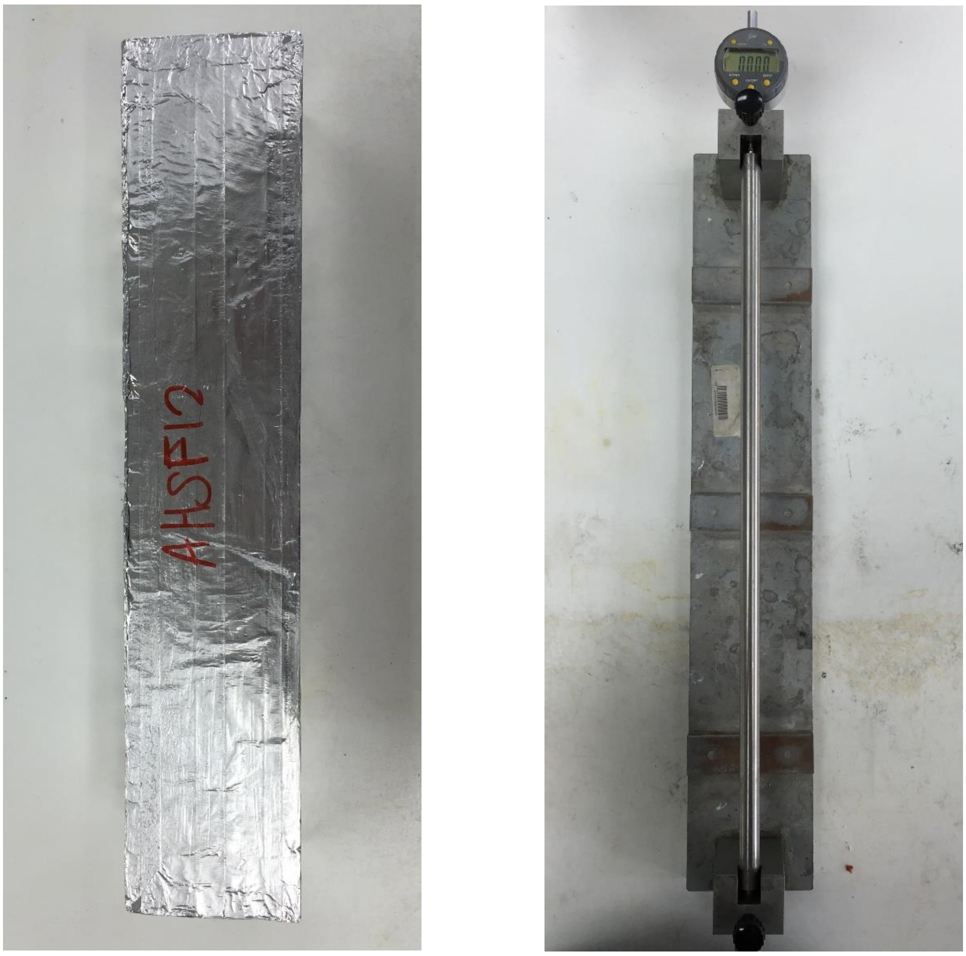

(a) *(b)*

Figure 9: (a) Shrinkage prism; (b) Shrinkage testing apparatus, including reference bar and mechanical displacement gauge

Void structure

Following strength testing, samples of each mix were used for image analysis of cross-sections. A GX microscope, with 1.3 mega pixel camera, was used to obtain focused images of void structures, laid out in Figure 15. The undefined colour of void boundaries prevented use of a computer program to identify void diameters, but since void numbers in each image were low and all voids approximately circular in 2D shape, the analysis was performed manually. In each image, a manual reference scale was incorporated, allowing subsequent void diameters to be scaled according to their pixel length.

4 Results and discussion

4.1 Compressive strength

Effect of composition

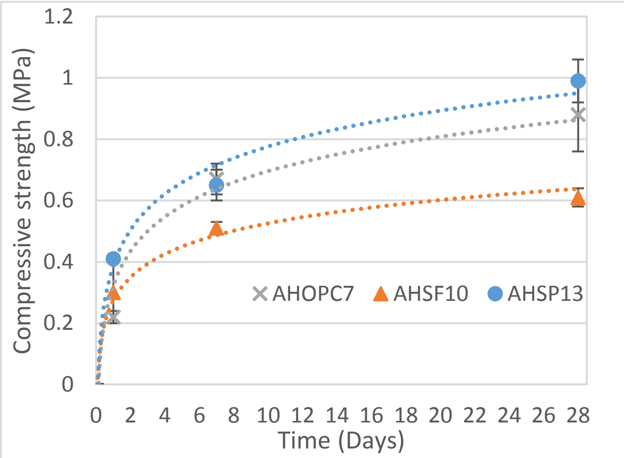

(a) 400 kg/m³

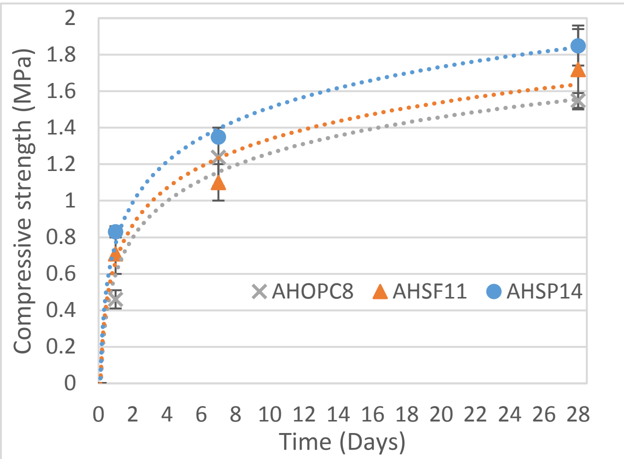

(b) 600 kg/m³

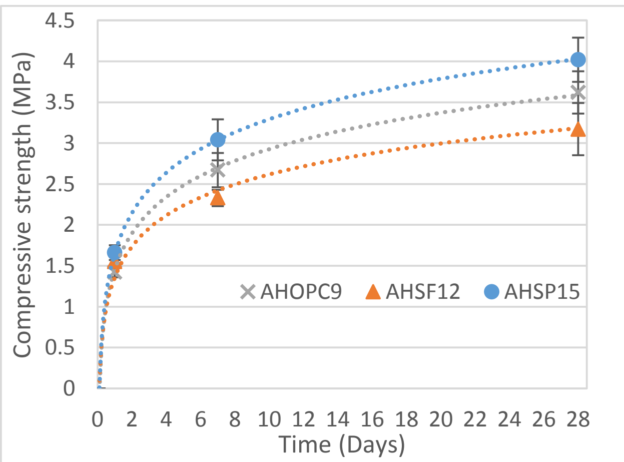

(c) 800 kg/m³

Figure 11: Compressive strength vs Time

Effect of density

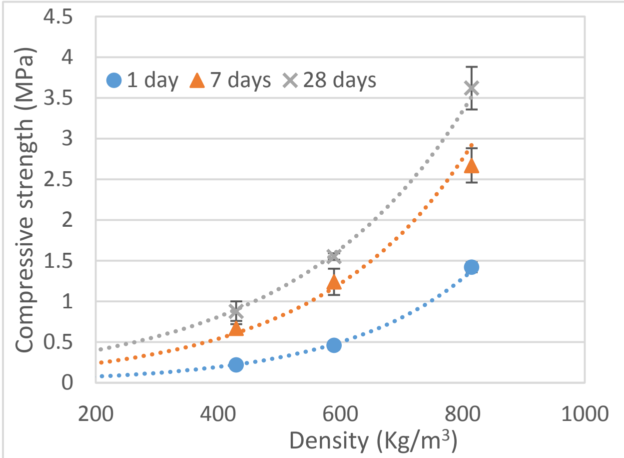

(a) AHOPC7 – 9: OPC only

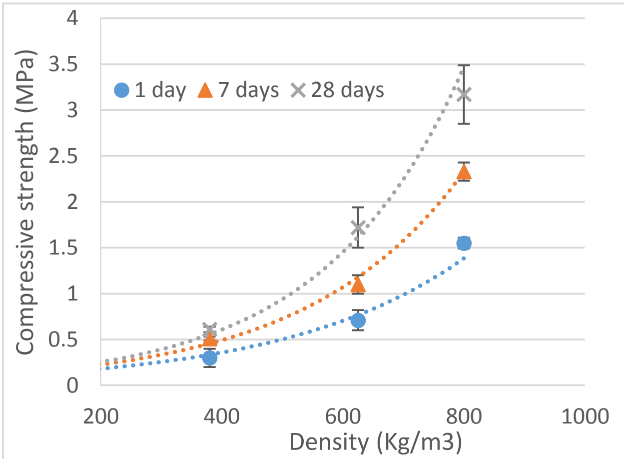

(b) AHSF10 – 12: OPC + SF

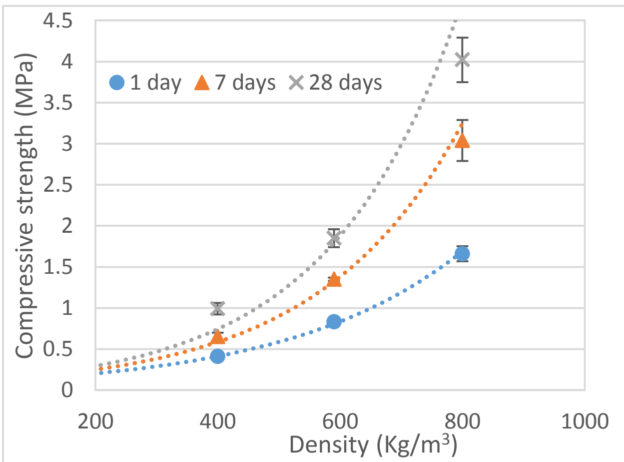

(c) AHSP13 – 15: OPC + SF + SP

Figure 10: Compressive strength vs Density

4.1.1 *Effect of composition*

The compressive strength results are detailed graphically in Figure 10, showing strength development with time for each density. All mixes show an approximately logarithmic strength development, where strength increases with time, but the rate of increase slows. At all densities of 400, 600 and 800kg/m^3, the replacement of 10% by weight of Portland cement with silica fume provides greater initial strength (1 day) than that of pure OPC. This is a result of the rapid pozzolanic reaction of silica fume with calcium hydroxide in the cement paste to produce CSH, the primary strength constituent in cements.

However, the replacement with silica fume seems to have a weakening effect for longer term strengths, showing pure OPC mixes to have greater long-term strength capacity. This is most exaggerated in mixes of density of 400kg/m^3 where the long-term strength of mixes containing silica fume was just 2/3 of the strength for pure OPC mixes. Whilst silica fume provides initial strengthening, perhaps the rapid structural development of the matrix provides less rigidity than when formed over a longer period of time. Furthermore, whilst the long-term strength of mix AHSF11 seems to defy this statement, there is considerable variation in the strength values recorded at 28 days, as shown by the large error bars attached to this data point.

In order to obtain greater initial strengths, the superplasticizer, Sika Viscocrete 10, was added in further cement replacement, leading to mixes AHSP13, AHSP14, and AHSP15. The results gave greater initial and long-term strengths at all densities than other mix compositions, as shown above in Figure 10. This can be attributed to the water-reducing capacity of superplasticizers, which allowed the water/binder ratio of the mix to be reduced to 0.4. Therefore, greater cement content at a given density is possible, since foam is less dense than water, and hence greater strength enhancement at all ages.

4.1.2 Effect of density

Figure 11 shows an underlying relationship of compressive strength increasing approximately exponentially with density for all mix compositions under investigation, and at each of the testing periods. 1 day and 7 day strengths follow the exponential curves most closely, and also have lower variation in recorded values, confirming a close fit.

The increasing rate of strength gain with density is in line with existing literature. Powers [46] showed empirically that compressive strength is proportional to the cube of cement gel/space ratio. This is in line with the results of Figure 11, since it suggests that higher gel/space ratios (i.e. higher densities) give higher strengths, and that the *rate of strength increase* increases with density.

Since density is closely aligned with porosity [19], several of the strength prediction models mentioned earlier are of interest for analysis. Closer analysis of the void structure to obtain porosity measurements can then be inputted into the models and provide indications of the effect of porosity, and hence density, on compressive strength.

Feret's model

Feret's model is a compressive strength prediction model that relates compressive strength to volumetric proportions of cement, water and air. Using the method outlined in the Mix design section, c, w and a are all theoretical values derived using the target density, water/binder ratio and specific gravities of mix constituents. Since the target density is the only variable, Feret's model therefore gives a prediction of compressive strength based on density for each mix composition. Feret's equation is defined as:

$$\sigma_y = K\left(\frac{c}{c+w+a}\right)^n \tag{3}$$

where c, w and a are the absolute volumetric proportions of cement, water and air, and K and n are empirical constants. Here, n=2 is used, on recommendation for normal-weight concrete [20].

Furthermore, by defining the x-axis as Feret's parameter (=c/(c + w + a)), the graphs of Figure 12 can be constructed to find the value of the constant K.

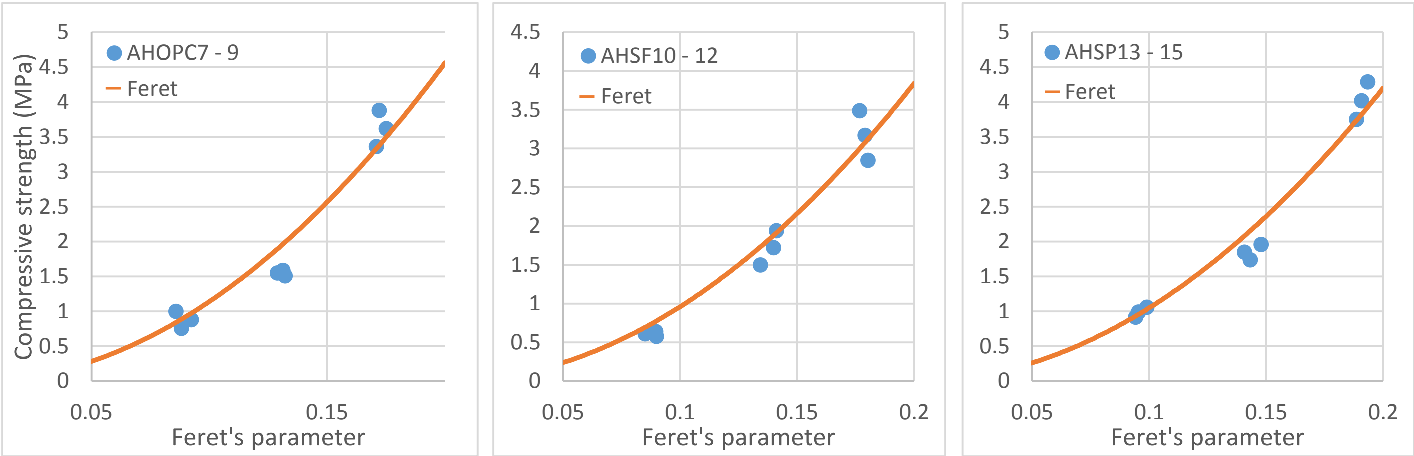

(a) *(b)* *(c)*

Figure 12: Compressive strength vs Feret's parameter for mixes (a) AHOPC7 – 9, (b) AHSF10 – 12 and (c) AHSP13 – 15

The values of K were found by plotting the empirical strength values against the square of Feret's parameter, and evaluating the gradient of the line of best fit through the points. The values of K are outlined below.

Mix	AHOPC7 – 9	AHSF10 - 12	AHSP13 - 15
K	114	96	105
R-squared	0.93	0.95	0.97

Table 2: Values of K and R-squared for Feret plots of AHOPC7 – 9, AHSF10 – 12 and AHSP13 – 15

All graphs from Figure 12 show that the empirical data is closely correlated with a second order curve of Feret's parameter. This is confirmed by the very high R-squared values in Table 2, which indicate a close fit between the curve and the data. Feret's curve provides the best fit for OPC + SF + SP mixes, AHSP13 – 15, with a value calculated for K of 105 and a high R-squared of 0.97. Nevertheless, since all mixes correlated closely, this indicates that compressive strength is very closely linked to density, regardless of mix composition.

4.1.3 Void structure

Following compressive strength testing, samples were analysed using microscopy to ascertain the size and distribution of voids within each mix. 9 microscope images were taken for each mix at systematic locations across the cross-section, as shown schematically in Figure 13, in order to gain a consistent representation across the sample.

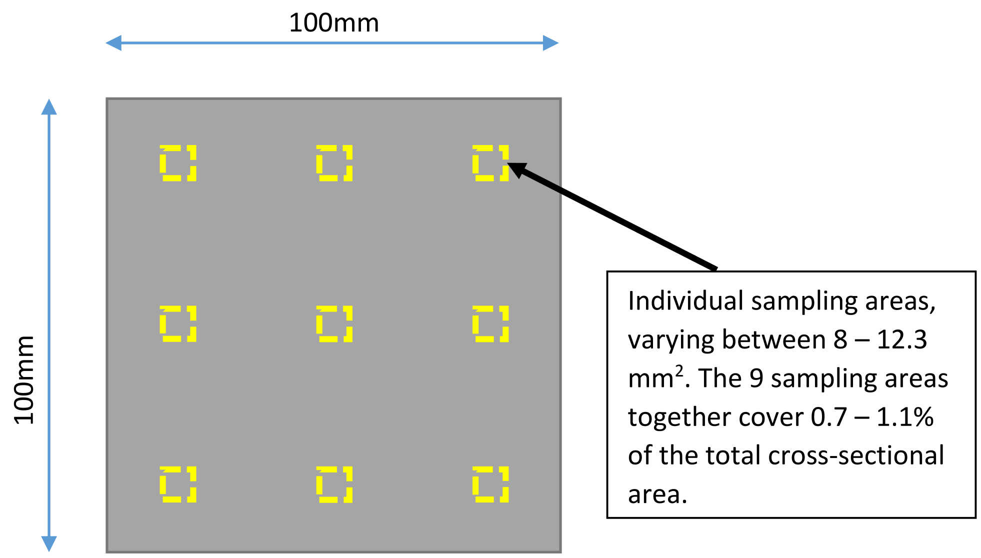

Figure 13: Schematic of location of sampling areas across cube cross-section

Following manual measurement of individual void diameters from the images, this data was statistically analysed to demonstrate the uniformity of void size distribution across the samples. The mean void diameter ($\bar{x}$), standard deviation (s), coefficient of variation (COV), and 95% Confidence Intervals were calculated for each sample size, n, using the following formulae:

$$\bar{x} = \frac{\sum_{i=1}^{n} x_i}{n} \quad (7)$$

$$s = \sqrt{\frac{\sum_{i=1}^{n}(x_i - \bar{x})^2}{n-1}} \quad (8)$$

$$COV = \frac{s}{\bar{x}} \quad (9)$$

$$\text{95\% Confidence Interval} = \left(\bar{x} \pm 1.96\frac{s}{\sqrt{n}}\right) \quad (10)$$

The standard deviation provides a value for absolute variation in void size, whilst the coefficient of variation gives the best measure of uniformity of voids across the sample, since it shows the *relative* void size variation compared to the mean.

Mix	AHOPC7	AHOPC8	AHOPC9	AHSF10	AHSF11	AHSF12	AHSP13	AHSP14	AHSP15
Mean void diameter (µm)	1205	742	657	965	861	655	1204	852	724
Standard deviation (µm)	816	272	301	426	366	269	597	285	331
CoV (%)	67.7%	36.7%	45.8%	44.1%	42.5%	41.1%	49.6%	33.4%	45.8%
Upper 95% CI (µm)	1423	793	740	1070	962	711	1363	918	794
Lower 95% CI (µm)	987	691	574	861	760	600	1045	786	653

Table 3: Statistical void size and distribution data for each mix

The data from Table 3 clearly shows the relationship between density and mean void diameter, with the lightest mixes (AHOPC7, AHSF10, AHSP13) having the largest voids. This is expected, given the higher foam volume within lower density mixes.

The lowest density mixes also exhibit the greatest void standard deviations and coefficient of variations, showing they have the greatest variation in void diameter and hence the poorest uniformity across the sample. This is likely to result from increased void coalescence at lower densities, since voids are typically larger and more closely spaced. Greater coalescence would then give considerable variation in void diameter, whilst maintaining the same void volume throughout the sample.

This is in line with statements from existing literature. Coalescence of air voids is stated to be due to differential surface tension between voids [47], which results from differential pressure on the water between voids. Differential surface tension is greatest between voids of large and small diameters. Therefore, this differential pressure leads to air of the smaller void diffusing through the surrounding water into the larger void, and hence coalescence as the smaller void is consumed. Such diffusion occurs more commonly in lower density mixes with voids of greater volume and closer spacing.

Furthermore, greater coalescence at lower density also explains why all mixes of the lowest target density have greater variation in mean void diameter than those of higher densities. For example, mixes of 400kg/m^3 have mean void diameters ranging from 965 – 1205μm, whilst for those of 800kg/m^3 the variation is just 655 - 724μm.

According to this data, all mixes fail to satisfy LOR's mean void size criteria of a diameter less than 500μm, which is also not contained within any of the 95% confidence intervals. The closest mix was AHSF12, with a mean diameter of 655μm and lower 95% confidence interval value of 600μm, which remains some way from the desired value. LOR's criteria is borne from the notion that the optimum void structure for maximum compressive strength is one of many small voids distributed uniformly across the sample [39]. However, in order to obtain low densities, this remains difficult, and highlights the challenge of LOR's criteria.

The limitation of this method is that the 2D cross-section analysed is highly unlikely to pass through the centre of a given void sphere. The resulting void circles shown on the 2D section are therefore almost certainly smaller in diameter than the void sphere, and so the estimated mean void diameters from Table 3 are underestimates. However, the extent of this underestimate can be determined from a rule of geometric probability for spheres. This states that for planes intersecting a sphere, the radius of the 2D void circles will have a probability density function of:

$$\phi_r = \frac{r}{R\sqrt{R^2 - r^2}} \tag{11}$$

where r is the radius of each profile circle, and R is the radius of the sphere [48]. This shows that circles of radii close to the sphere radius have the greatest probability of occurring. Therefore, it can be concluded that the observed 2D void circles are likely to be close in diameter to the void sphere diameter, and so the mean void diameters shown in Table 3 are only small underestimates. This justifies the accuracy of the void size and distribution results obtained from statistical analysis of each mix. This limitation does not apply to the calculation of void area fractions from a 2D section, to be discussed below.

Stereological analysis and Balshin's model

Stereological analysis involves the application of properties derived from two-dimensional cross-sections to the three-dimensional material. The theory is based on Delesse's principle, which shows that for a random plane section through an isotropic material, the area fraction of a phase in the 2D section is equal to the volume fraction in the 3D space [49]. Here, the void area fraction has been calculated from sample microscopy images of each mix, and by stereology is equivalent to the volume fraction of voids in the 3D cube, and hence porosity of the sample. These values are outlined in Table 4 below.

Mix	AHOPC7	AHOPC8	AHOPC9	AHSF10	AHSF11	AHSF12	AHSP13	AHSP14	AHSP15
Void area	89.3	53.4	59.6	55.8	53.4	35.4	76.3	44.9	42.2
Sampling area	110.7	77.7	108.7	75.3	79.2	79.1	91.1	71.8	79.4
Porosity	80.7%	68.7%	54.9%	74.1%	67.4%	44.7%	83.8%	62.6%	53.2%

Table 4: Porosity calculations for each mix

Using the calculated porosities, Balshin's strength-porosity model, $\sigma_y = \sigma_0(1-n)^b$, can be fitted to empirical values on a strength vs porosity graph. This provides estimate values of the unknown constants, σ_0 and b, for the different mix designs considered. Figures 14(a) and 14(b) display the approximations for OPC + SF mixes, AHSF10 – 12, and OPC + SF + SP mixes, AHSP13 – 15, respectively.

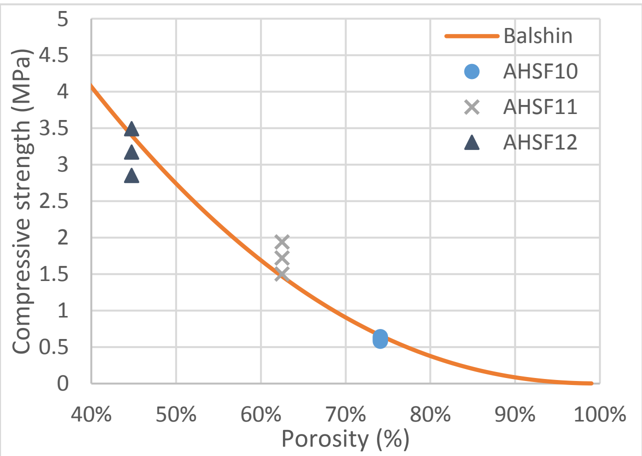

(a) AHSF10 – 12: OPC + SF

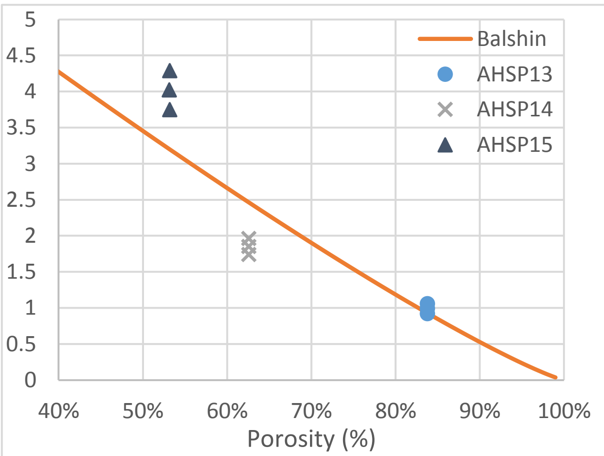

(b) AHSP13 – 15: OPC + SF + SP

Figure 14: *Compressive strength vs porosity for mixes (a) AHSF10 – 12, (b) AHSP13 – 15*

By taking logs of Balshin's equation to produce equation (12), a linear curve can be plotted through the empirical data points.

$$\ln \sigma_y = \ln \sigma_0 + b \ln(1-n) \qquad (12)$$

The values of σ_0 and b are then obtained using the gradient and y-intercept of the line that most closely fit the data. The R-squared statistic quantifies the adequacy of the curve as a fit to the data.

The values obtained are summarised in Table 5 below, and used in the plots of strength against porosity in Figure 14.

Mix	σ_0	b	R-squared value
AHSF10 – 12	12.3	2.2	0.96
AHSP13 – 15	7.8	1.2	0.85

Table 5: Values of σ_0, b, and R-squared for Balshin plots of AHSF10 – 12 and AHSP13 – 15

Balshin's model therefore provides an excellent fit for mixes containing silica fume, AHSF10 – 12, since a high R-squared value of 0.96 is obtained. The value of b, 2.2, is lower than that used by Hoff for mixes containing only air, water and cement, thus indicating a steeper strength-porosity relationship. This is counteracted, however, by a decrease in σ_0, the theoretical strength at zero porosity, to produce strengths that are lower than those of pure OPC mixes at all densities. Whilst silica fume has the effect of increasing *initial* strength at all densities, Balshin's model therefore confirms that a binder matrix of 100% OPC produces greater *long-term* strengths.

The graphs also show that whilst the addition of superplasticizer further reduces σ_0, this is more than counteracted by a significant decrease in the power coefficient b, which produces a very steep strength-porosity relationship. This is likely to result from the water-reducing capacity of the superplasticizer, which allows greater cement paste for a given porosity, and hence greater compressive strength capacity.

It should be noted that Balshin's model is applicable for long-term strengths only. Here, long-term strength has been approximated as 28-day strength, which may not be entirely accurate. According to earlier Figure 10, all strength curves have positive gradients at 28 days, and so have not reached full strength development. This is a small point, however, since all curves appear close to their plateaus, and so the coefficients calculated for Balshin's model are accurate.

Hoff's application of Balshin's model to mixes containing only air, water and cement, using a theoretical density, yielded values for σ_0 of 115 – 290 MPa, and for b of 2.7 – 3. For 400 kg/m^3, the measured value of 0.88MPa lies just greater than Hoff's values of 0.55 – 0.76MPa, whilst at 600 kg/m^3 the measured value of 1.55MPa is just below Hoff's range of 1.64 – 2.57MPa. At 800 kg/m^3, the measured 3.62MPa is within Hoff's range of 3.55 – 6.10MPa. Therefore, we can say that, for our mixes, Hoff's model improves at higher densities.

Hoff's model would be expected to give slightly higher strength values than those measured at 28 days, since it assumes an average value of 0.2 for the proportion of water bound by hydration to cement (by weight). This ratio would be expected to be smaller at 28 days since hydration is at an earlier stage, which would thus increase Hoff's theoretical porosity leading to a decrease in true predicted strength.

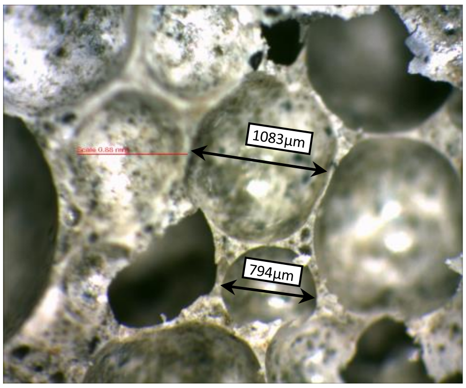

(a) AHOPC7

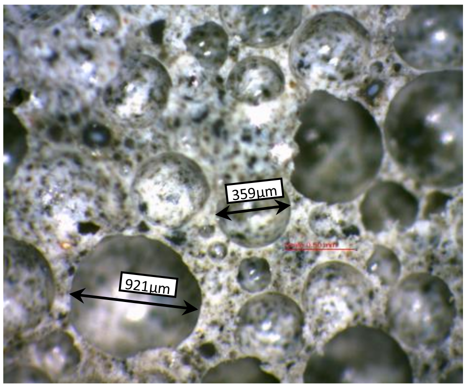

(b) AHOPC8

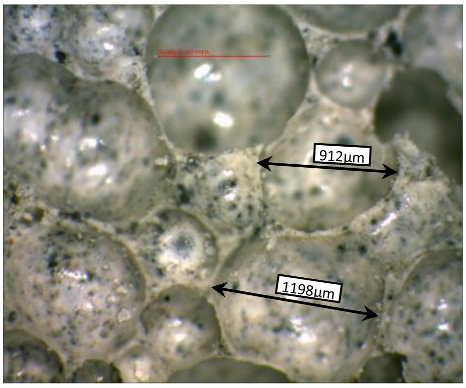

(c) AHSF10

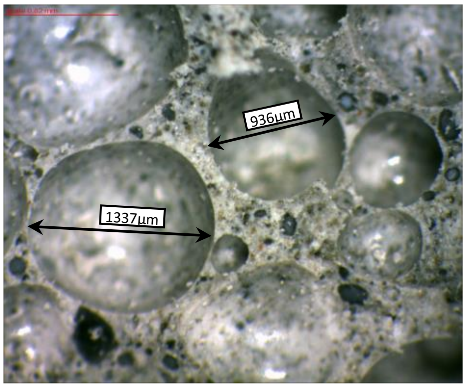

(d) AHSF11

(e) AHSF12

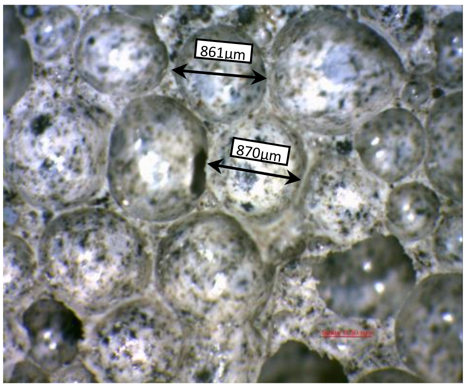

(f) AHSP13

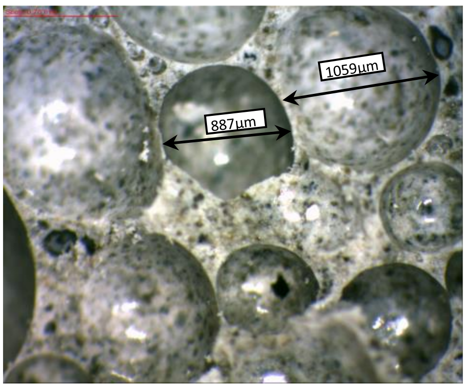

(g) AHSF14

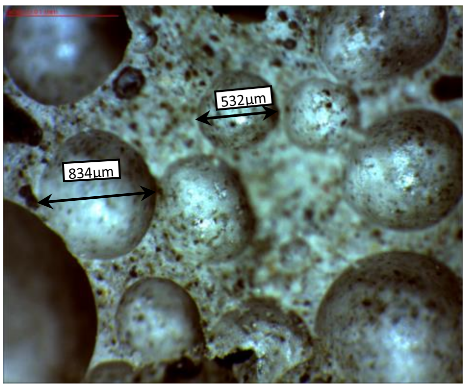

(h) AHSF15

Figure 15: Microscope images of the mixes' void structure

4.2 Autogenous shrinkage

4.2.1 Effect of composition

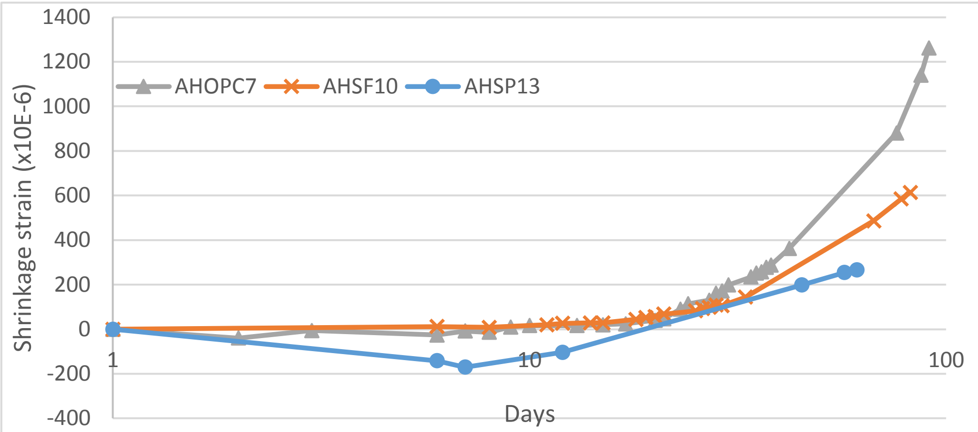

(a) 400 kg/m³

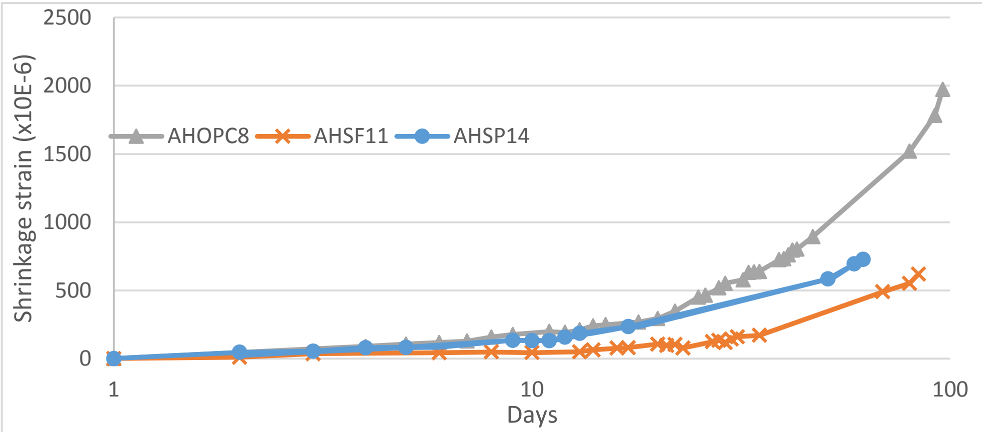

(b) 600 kg/m³

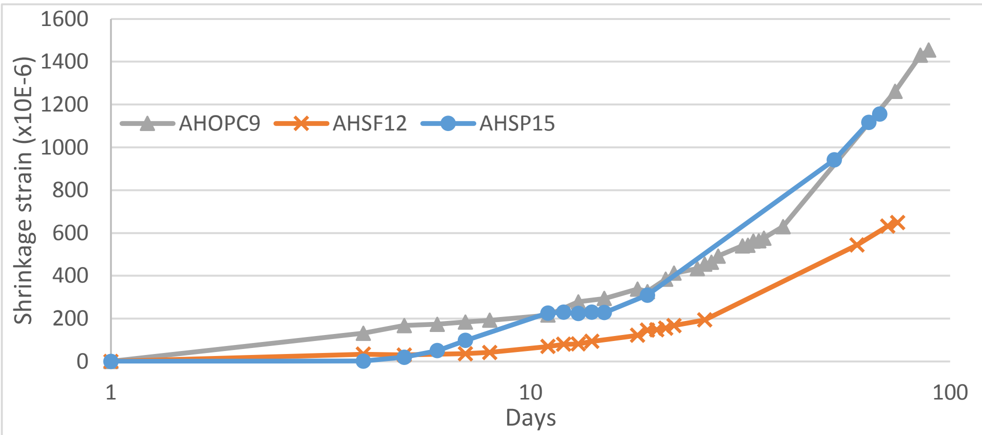

(c) 800 kg/m³

Figure 16: Autogenous shrinkage strain vs time at (a) 400 kg/m³, (b) 600 kg/m³ and (c) 800 kg/m³

Typical values of autogenous shrinkage strain for normal weight concrete are 40 x 10^{-6} at the age of 1 month [13]. In this study, observed values at 1 month are up to 50 times this amount. This highlights the significance of autogenous shrinkage within foamed concrete applications.

Figures 16 and 17 show autogenous shrinkage strain increasing with time for all mixes. Linear time scales show strain to increase linearly with time, although a log scale is used to more clearly differentiate data recorded at early intervals.

Figure 16 shows that the addition of silica fume significantly reduces shrinkage at all times relative to OPC mixes. The effect becomes clearer for higher densities, where the disparity between OPC and OPC + SF lines becomes greater. Furthermore, at densities of 600 kg/m^3 and 800 kg/m^3, the addition of silica fume also appears to retard a sharp onset of shrinkage on the log scale. Both factors are, in fact, a reflection of the greater difference in *linear* gradients between the OPC and OPC + SF mixes at higher densities. This suggests that OPC content is a primary driver behind shrinkage strain of foamed concrete. At 400 kg/m^3, the OPC + SF mix, AHSF10, increases in gradient on the log scale simultaneously with AHOPC7, reflecting a smaller difference in linear gradient. Perhaps at such a low density, the small OPC replacement by silica fume is insufficient to highlight sufficient difference in shrinkage, particularly at early ages.

The addition of superplasticizer at all densities increases shrinkage relative to OPC + SF mixes. This is due to the lower water/binder ratio employed. At lower water/binder ratios, a greater proportion of water is required for earlier hydration, and the lack of availability in later hydration leads to the formation of capillary tubes. The development of fluid surface tension within these capillary tubes then leads to increased autogenous shrinkage at earlier ages.

At a density of 400 kg/m^3, the AHSP13 mix shows early signs of small volume expansion up to 8 days, beyond which positive shrinkage strain ensues. This may be due to the lower water content providing a more optimal value for initial cement hydration at this density, leading to greater heat generation and thermal expansion. At day 8, however, it appears that normal autogenous shrinkage has increased sufficiently such that it offsets the expansion, and positive shrinkage values ensue. Nevertheless, the continued thermal effects mean that the gradient of AHSP13 remains lower than that of AHSF10.

Despite increased shrinkage due to the addition of superplasticizer, mixes AHSP13 and AHSP14 show shrinkage magnitudes lower than those of pure OPC binders, whilst AHSP15 has values approximately equal. This suggests that the composition including both silica fume and superplasticizer is promising for future development of foamed concrete since it also showed greater strengths than OPC mixes for all densities at all ages.

4.2.2 Effect of density

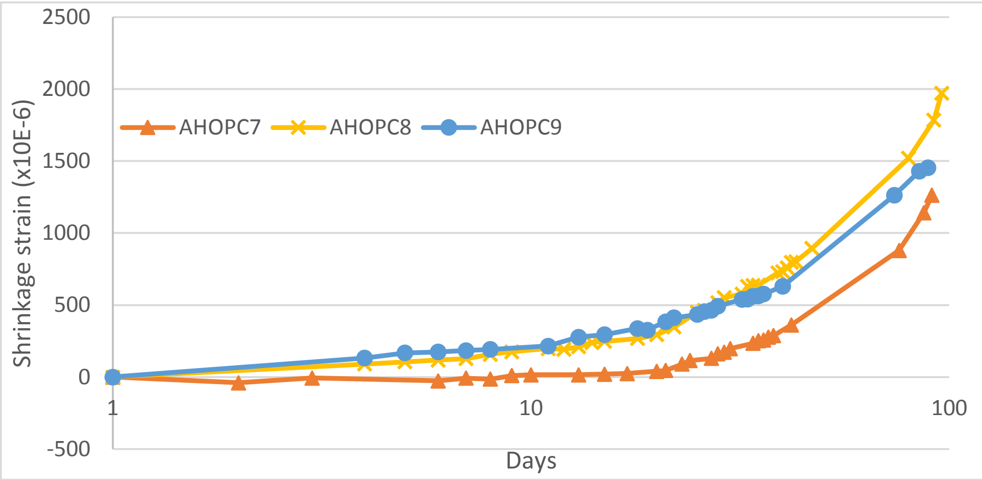

(a) AHOPC7 – 9: OPC only

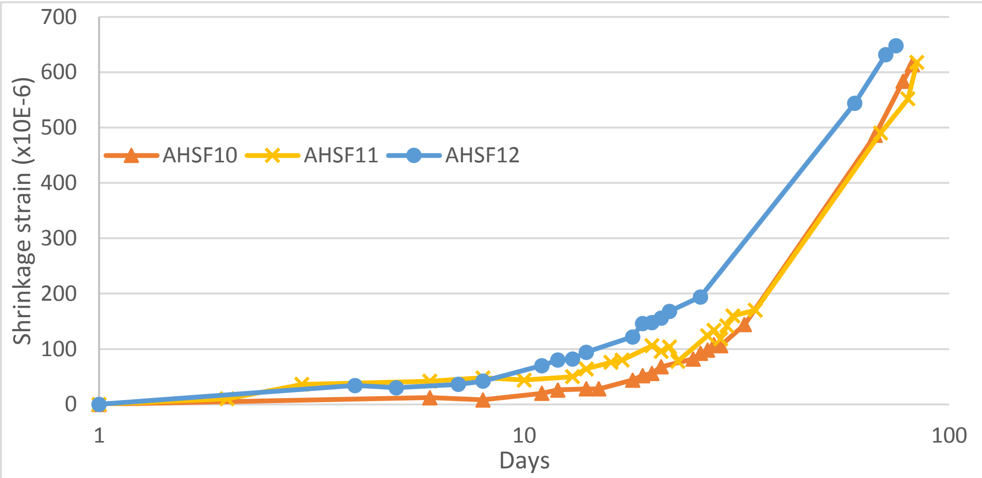

(b) AHSF10 – 12: OPC + SF

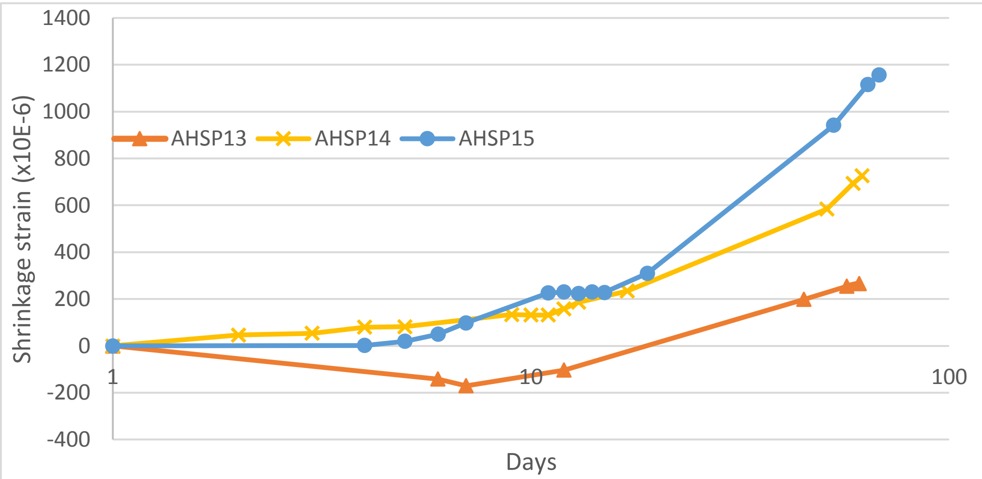

(c) AHSP13 – 15: OPC + SF + SP

Figure 17: Autogenous shrinkage strain vs time for (a) AHOPC7 – 9, (b) AHSF10 – 12 and (c) AHSP13 – 15

From Figure 17, autogenous shrinkage strain increases with density for all mixes. In each graph, the sharp increase in gradient for lighter mixes occurs later than that of heavier mixes. This reflects the greater linear gradient of heavier mixes, and shows heavier mixes to undergo greater shrinkage. This is in line with literature, which suggests autogenous shrinkage strain increases with greater cement content [13] (i.e. higher density). The exception to this is the curve of AHOPC9, the heaviest mix for OPC binders, which lies slightly below that of AHOPC8 in the latter regions (days > 40).

Whilst the gradients for OPC and OPC + SF mixes appear similar for each density, there is significant disparity between those observed for OPC + SF + SP mixes, with AHSP15 increasing at a rate far greater than that of AHSP13. This suggests that higher cement content not only increases shrinkage by itself, but also enhances the effect of other shrinkage-influencing factors, in this case the reduction in water/binder ratio.

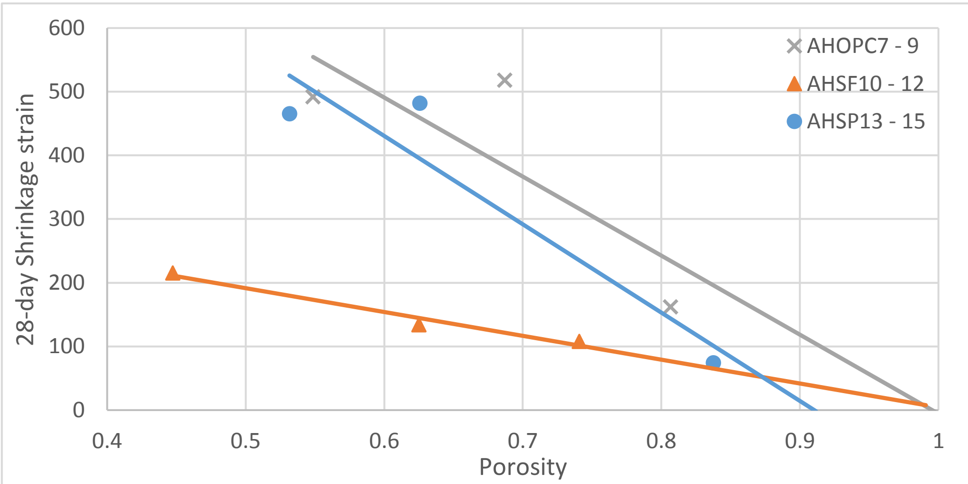

Figure 18: 28-day shrinkage vs porosity for all mixes

Figure 18 summarises the above analysis using an arbitrary shrinkage value at 28 days: shrinkage strain decreasing with increasing porosity (decreasing density), and OPC mixes demonstrating the greatest shrinkage strains at all porosities.

5 Conclusions and further work

The main findings of this study are summarised as follows:

1. Silica fume addition increases early strength at all densities, but reduces long-term strengths relative to OPC mixes.
2. Superplasticizer addition can increase both initial and long-term strengths at all densities. Superplasticizers allow the reduction in water/binder ratio, which increases strength due to greater cement content.
3. Density is the primary factor influencing strength at low densities: Compressive strength increases approximately exponentially with density for all mix compositions analysed, whilst strength variation between mixes also appeared to increase at higher densities.
4. Feret's model provides an accurate prediction of compressive strength for all mix compositions analysed based on volumetric proportions of cement, water and air.
5. Void sizes were narrower and more uniformly distributed for mixes of higher density. The mix composition did not appear to affect void distribution.
6. Balshin's strength-porosity model provides an accurate prediction of compressive strength for OPC + SF mixes. The model is considerably less valid for OPC + SF + SP mixes, however. Hoff's application of Balshin's model to OPC mixes is more accurate at higher densities.
7. Cement replacement by silica fume reduces shrinkage strain at all densities. The reduction in water/binder ratio due to superplasticizer addition increases shrinkage strain, although this remained lower than that of OPC mixes.
8. Shrinkage strain is greater at higher densities due to greater cement content.

This study developed a foamed concrete mix with optimised early strength at low densities relative to an OPC mix. Whilst the advantageous properties of workability, thermal insulation and void filling ability are well documented, this study has demonstrated the versatility of foamed concrete, since the strengths of the OPC + SF + SP mix at 800 kg/m^3 are now comparable to those of lightweight aggregate concrete. Whilst further optimisation is necessary before commercial use, it is hoped that this work will contribute towards the development of foamed concrete for more diversified applications, whereby the lightweight, rapid early strength properties can be exploited. These may include rapid void filling to prevent structural collapse, or the fast provision of insulation through temporary relief shelters.

Compliance with Laing O'Rourke specification

LOR Specification	**1** Density < 800 kg/m^3	**2** LT strength > 4MPa	**3** Void size < 0.5mm	**4** Expansion ≈ 0.5%	**5** Early strength ≥ 25% LT	**6** Closed voids
AHOPC7	**430**	22%	241%	-ve	**25%**	Not tested, but visual inspection indicated closed voids
AHOPC8	**590**	39%	148%	-ve	**30%**	
AHOPC9	815	91%	131%	-ve	**39%**	
AHSF10	**380**	15%	193%	-ve	**49%**	
AHSF11	**625**	43%	172%	-ve	**41%**	
AHSF12	**800**	79%	131%	-ve	**49%**	
AHSP13	**400**	25%	241%	-ve	**41%**	
AHSP14	**590**	46%	170%	-ve	**45%**	
AHSP15	**800**	**101%**	145%	-ve	**41%**	

Table 6: A summary of mix properties according to LOR's specification. Percentages indicate the proportion of specified value observed, whilst bold numbers indicate that the specification was satisfied

The mixes analysed proved successful in satisfying LOR's early strength criteria, and also met long-term strength requirements in one case. Void sizes were close at higher densities, whilst shrinkage was expected to fall short since expansive agents were not utilised. The interconnectivity of voids was not quantitatively assessed, but visual inspection indicated that voids were closed and spherical in shape.

All mixes met specification 1 requiring densities less than 800 kg/m^3, except AHOPC9, which had a mean density of 815 kg/m^3. This, however, is a small deviation from the target density, and within the accepted industry tolerance of ±50 kg/m^3 [35], and so considered acceptable.

Specification 2, which required a long-term strength of 4MPa, was satisfied by only AHSP15, which contains both silica fume and a superplasticizer, and is at the higher density of 800 kg/m^3. However, strength development is likely to continue beyond 28 days, and so AHOPC9 may also satisfy the specification if a later value of long-term strength was assessed. Since prior analysis indicated the strong relationship between compressive strength and density, it is unsurprising that all mixes at the lower densities 400 kg/m^3 and 600 kg/m^3 did not satisfy the criterion.

There was considerable deviation between the required and observed values for specification 3, with only void sizes for mixes of 800 kg/m^3 close to meeting the required value of 0.5mm. Furthermore, since spherical void sizes were based on a 2D cross-section, it is highly likely that the average void size was underestimated. As such, true values from all mixes can be considered significantly greater than the specified void size.

The lightly expansive (≈ 0.5%) requirement of specification 4 was not expected to be satisfied by any mix, since no expansive agent was utilised, and thus positive shrinkage values were observed in all cases. The study aimed to reduce shrinkage rather than achieve expansion. This was achieved using the OPC + SF + SP composition, which produced shrinkage strains lower than OPC mixes at all densities.

Specification 5 required 1 day strengths greater than 25% of long-term strengths, and was satisfied by all mixes. The addition of silica fume greatly increased early strength at all densities, with values as high as 49% being reached. Given that only one mix achieved specification 2’s long-term strength requirement, and that the majority of mixes achieved the early strength target by a considerable margin, there may be an optimum midpoint whereby some early strength is sacrificed to promote long-term strength. This may be achieved through the pozzolanic reaction of fly ash.

Specification 6 was difficult to quantify using microscopy images, but it was generally observed that voids were not interconnected, and almost always spherically shaped. This is important in the prevention of water absorption, which can lead to freeze-thaw degradation, or the transportation of deleterious substances.

Further work

Additional work could focus on optimising the OPC + SF + SP mix with a view to satisfying LOR's criteria for shrinkage, void size and water absorption. Given that LOR's early strength criteria was comfortably satisfied at all densities, the replacement of a proportion of silica fume with an expansive agent, such as MgO, in combination with OPC and a superplasticizer could be investigated. The effect of decreasing the water/binder ratio could also be considered further, since further strength gains may be possible, although this should be considered alongside flowability.

Limited work on the effect of curing regime on foamed concrete has been carried out. In particular, this work could consider the effect of temperature on hydration, with a view to enhancing early and long-term strengths. Further work could also be performed on the use of fibre reinforcement in foamed concrete. This may be used to reduce shrinkage cracking, but its effect on compressive strength could also be analysed.

6 References

[1] The Concrete Society (2009). *Good Concrete Guide 7: Application and Specification*

[2] OECD (2012). *OECD Green Growth Studies*

[3] Brady K C, Watts G R A, Jones M R R (2001). *Specification for foamed concrete*

[4] Amran Y H M, Farzadnia N, Ali AAA (2015). *Properties and applications of foamed concrete; a review*

[5] Limbachiya M C, Kew H Y (2008). *Excellence in concrete construction through innovation*

[6] Kearsley E P (1996). *The use of foamed concrete for affordable development in third world countries*

[7] Visagie M, Kearsley E P (2002). *Properties of foamed concrete as influenced by air-void parameters*

[8] Nambiar E K K, Ramamurthy K (2007). *Air-void characterization of foamed concrete*

[9] Nambiar E K K, Ramamurthy K (2006). *Models relating mixture composition to the density and strength of foam concrete using response surface methodology*

[10] Nambiar E K K, Ramamurthy K (2006). *Influence of filler type on the properties of foam concrete*

[11] Sharma U, Khatriband A, Kanoungo A (2014). *Use of Microsilica as Additive to Concrete-state of Art*

[12] Bing C, Zhen W, Ning L (2012). *Experimental research on properties of high-strength foamed concrete*

[13] Neville A M (2011). *Properties of concrete*

[14] Jones M R, McCarthy A (2006). *Heat of hydration in foamed concrete: effect of mix constituents and plastic density*

[15] Kearsley E P, Wainwright P J (2001). *The effect of high fly ash content on the compressive strength of foamed concrete*

[16] Richard A O, Ramli M B (2014). *The Effects of Curing Methods on Early-age Strength of Sustainable Foamed Concrete*

[17] Hoff G C (1972). *Porosity-strength considerations for cellular concrete. Cement and Concrete Research*

[18] Nambiar E K K, Ramamurthy K (2008). *Models for strength prediction of foam concrete*

[19] Kearsley E P, Wainwright P J (2002). *The effect of porosity on the strength of foamed concrete*. Cem Concr Res; 32: 233 – 9

[20] Tam C T, Lim T Y, Ravindrarajah R, Lee S L (1987). *Relationship between strength and volumetric composition of moist-cured cellular concrete*. Mag Concr Res; 39:12 – 8

[21] Ali K, Gelim M (2011). *Mechanical and Physical Properties of Fly Ash Foamed Concrete*

[22] Jones M R, McCarthy M J, McCarthy A (2003). *Moving fly ash utilization in concrete forward: a UK perspective*

[23] Ziembicka H (1977). *Effect of micropore structure on cellular concrete shrinkage*

[24] Valore R C (1954). *Cellular concrete part 1 composition and methods of production. ACI J*

[25] Ramamurthy K, Narayanan N (2000). *Influence of composition and curing on drying shrinkage of aerated concrete*

[26] Kjellsen K, Atlassi E (1999). *Pore structure of cement silica fume systems - Presence of hollow shell pores*. Cement and Concrete Research, P133 – 142

[27] Boon K H, Loon L Y, Chuan D Y E (2006). *Compressive strength and shrinkage of foamed concrete containing pulverized fly ash*

[28] Weigler H, Karl S (1980). *Structural lightweight aggregate concrete with reduced density Lightweight aggregate foamed concrete*

[29] Ahmadi J, Naghdi R (2013). *Evaluation of autogenous shrinkage in high-performance concrete*

[30] Brooks J J, Cabrera J G (1998). *Factors affecting the autogenous shrinkage of silica fume high-strength concrete*. Proceedings of International Workshop on Autogenous Shrinkage of Concrete, Japan Concrete Institute, P185 – 192

[31] Zhang M H, Tam C T, Leow M P (2003). *Effect of water-to-cementitious materials ratio and silica fume on the autogenous shrinkage of concrete*

[32] Aldridge D, Ansell T (2001). *Foamed concrete: production and equipment design, properties, applications and potential*

[33] Shrivastava O P (1977). *Lightweight aerated concrete – a review*. Indian Concr J 1977; 51:10 – 23

[34] Weigler H, Karl S (1980). *Structural lightweight aggregate concrete with reduced density – lightweight aggregate foamed concrete*. Int J Lightweight Concr; 2:101 – 4

[35] Jones MR, McCarthy A (2005). *Preliminary views on the potential of foamed concrete as a structural material*

[36] Valore R C (1954). *Cellular concrete: Part 2 – physical properties*. ACI Journal

[37] Malhotra V (2004). *Role of Supplementary Cementing Materials and Superplasticizers in Reducing Greenhouse Gas Emissions.* Proceedings of ICFRC International Conference on Fiber Composites, High-Performance Concrete, and Smart Materials, Chennai, India, P489-499.

[38] Verma A, Chandak R, Yadav R K (2012). *Effect of micro silica on the strength of concrete with ordinary Portland cement*

[39] Hilal A A, Thom N H, Dawson A R (2014). *Effect of additives on void structure of foamed concrete*

[40] Aitcin P, Jolicoeur C, Macgregor J (1994). *Superplasticizers: How they work and why they occasionally don't*

[41] Alawode O, Dip P G, Idowu O I (2011). *Effect of Water/Cement Ratios on the Compressive Strength and Workability of Concrete and Lateritic Concrete Mixes*

[42] Verhasselt A, Pairon J (1989). *Rapid Methods of Distinguishing Plasticizer from Superplasticizer and Assessing Superplasticizer Dosage*

[43] Ramamurthy K, Nambiar E K K, Ranjani G I S (2009). *A Classification on Studies of Foam Concrete*

[44] Limbachiya M C, Kew H Y (2008). *Excellence in Concrete Construction through Innovation*

[45] Lamond J F (2006). *Significance of Tests and Properties of Concrete and Concrete-making Materials*

[46] Powers T C (1958). *Structure and Physical Properties of Hardened Portland Cement Paste*

[47] Wee T, Babu D S, Tamilselvan T, Lim H (2006). *Air-Void System of Foamed Concrete and its Effect on Mechanical Properties*

[48] Fonseca P C, Scherer G W (2014). *An image analysis procedure to quantify the air void system of mortar and concrete*

[49] Baddeley A, Vedel Jensen E B (2004). *Stereology for Statisticians*

7 Appendix

7.1 Risk assessment retrospective

The Risk Assessment performed prior to experimental work provided an accurate representation of the risks encountered. The majority of all risks identified were correctly mitigated against, although for some there was insufficient foresight as to when they would occur, whilst several unexpected risks also materialised.

The risk of dust inhalation was a prominent risk that occurred more often than anticipated. For example, during both the placing of dry cement into the mixer, and the initial mixing of dry constituents, significant amounts of dust were expelled through the mouth of the mixer. As a result, a rubber mat had to be placed over the mouth of the mixer in order to retain all dust in the mixing process. The mat was also employed upon the initial addition of water for higher density mixes with greater cement and water contents, since the greater volume of material within the mixer occasionally led to some liquid being expelled.

The distance of the concrete laboratory, where mixing was performed, from the constant temperature room meant there was a significant amount of manual transportation of materials, shrinkage specimens and moulds. Whilst logistically unavoidable, several of these items had to be carried by hand in order to reduce vibration, and so provided significant risk of injury if performed by a single person. Ideally, the concrete mixing lab would also be kept at a constant temperature and relative humidity, allowing curing to occur there and removing the need to transport heavy and delicate items over long distances.

An unanticipated risk was the generation of excess foamed concrete in the mixing process, and its subsequent disposal. The difficulty in meeting the target density, particularly with mixes containing a superplasticizer, meant that occasionally several additional litres remained following pouring. The hazardous nature of liquid foamed concrete thus required full compliance with COSHH procedures. The material was separated from the environment by placing it in sealed plastic bags and being left to set in a designated area, before disposal into a skip.

This Risk Assessment was built upon that of a similar experimental procedure carried out previously. For future experiments, this augmentation should continue in order to provide the most comprehensive review of the associated risks.